Experimental determination of activities of FeO and Fe2O3 components in hydrous silicic melts under oxidizing conditions.

Fabrice Gaillard, Michel Pichavant, Bruno Scaillet

Experimental determination of activities of FeO and Fe_2O_3 components in hydrous silicic melts under oxidizing conditions

Fabrice Gaillard[1], Michel Pichavant[1,] and Bruno Scaillet[1]

[1] Institut des Sciences de la Terre d'Orléans (ISTO), UMR 6113, 1A rue de la Férollerie, Orléans cedex 02 45071, France

Abstract

The critical role of iron on crystal-silicate liquid relationships and melt differentiation is mainly controlled by the redox conditions prevailing in magmas, but the presently available database merely constrains the thermodynamic properties of iron-bearing components in strongly reduced and anhydrous molten silicate where iron is in the ferrous form. This paper provides new standard states for pure ferrous (FeO^{liq}) and ferric ($Fe_2O_3^{liq}$) molten iron oxides and extends the experimental database towards oxidizing and water-bearing domains. Iron-iridium, iron-platinum alloys, magnetite or hematite were equilibrated with synthetic silicic liquids at high temperature and high pressure under controlled oxygen fugacity (fO_2) to determine activity-composition relationships for FeO^{liq} and $Fe_2O_3^{liq}$. Between 1000 and 1300°C, the fO_2 ranges from that in air to 3-log units below that of the nickel-nickel oxide buffer (NNO). Experiments were performed on both anhydrous and hydrous melts containing up to 6-wt.% water. Incorporation of water under reducing conditions increases the activity coefficient of FeO^{liq} but has an opposite effect on $Fe_2O_3^{liq}$. As calcium is added to system, the effect of water becomes weaker and is inverted for $Fe_2O_3^{liq}$. Under oxidizing conditions, water has a negligible effect on both activities of FeO^{liq} and $Fe_2O_3^{liq}$. In contrast, changes in redox conditions dominate the activity coefficients of both FeO^{liq} and $Fe_2O_3^{liq}$, which increase significantly with increasing fO_2. The present results combined with the previous work provide a specific database on the energetics of iron in silicate melts that cover most of the condition prevailing in natural magmas.

1. Introduction

The construction of thermodynamic models for multicomponent melts and magmas represents an important direction of research in petrology. Calibration of such models requires determination of both standard states and mixing properties for the melt components. Presently, the most abundant source of data constraining the mixing properties of silicate melts is phase equilibria [Berman and Brown, 1987], as illustrated by several models (e.g., [Berman and Brown, 1984, Eriksson and Pelton, 1993, Ghiorso and Sack, 1995 and Kirschen and Pichavant, 2001]. To test and verify predictions of these models and to provide supplementary constraints for the calibration of the mixing relationships of multicomponent silicate melts, additional measurements such as determinations of activities of the melt components are needed.

Among the different components to be considered, the iron oxide melt components are critical because both ferric and ferrous iron exist in different proportions in magmas, depending on fO_2, P, T and chemical composition (e.g., [Thornber et al., 1980, Mysen and Virgo, 1989, Kress and Carmichael, 1991 and Gaillard et al., 2001]). In the literature of material science,

numerous studies on the energetics of iron in molten silicate were performed on synthetic systems that are, however, very different from natural magmas compositions [Matsuzaki et al., 1998]. Surprisingly, despite the fact that iron is the most abundant multivalent element present in magmas, the thermodynamic behavior of other easily reducible cations such as Ni or Co has retained more attention in the geological literature [O'Neill and Eggins, 2002]. Also, the presently available database is mostly devoted to the thermodynamic properties of iron in strongly reduced and anhydrous molten silicate where iron is in the ferrous form [Doyle and Naldrett, 1986]. Changes in ferric-ferrous ratio have important effects on Fe-Ti oxide saturation curves [Osborn, 1959 and Hamilton et al., 1964]. The position of Fe-Ti oxides in the crystallization sequence controls the iron content (and ferric-ferrous ratio) of the residual melt, and consequently the stability and composition of major silicate phases [Sisson and Grove, 1993, Martel et al., 1999 and Pichavant et al., 2002]). Fe-Ti oxides can be near-liquidus phases in basalt for fO_2 above the nickel-nickel oxide buffer (NNO) under hydrous conditions [Hamilton et al., 1964, Sisson and Grove, 1993, Martel et al., 1999 and Pichavant et al., 2002]. Conversely, under anhydrous and reducing conditions, Fe-Ti oxides crystallize near the solidus [Lapin et al., 1985, Snyder et al., 1993 and Toplis and Carroll, 1995]. For modeling Fe-Ti oxide saturation and liquid lines of descent, an accurate calibration of the thermodynamic properties of ferrous and ferric iron in multicomponent melts is therefore needed. The phase equilibria calculated from models presently available do not reproduce accurately experimental Fe-Ti oxide saturation curves [Ghiorso and Sack, 1995, Toplis and Carroll, 1996 and Ariskin, 1999]. This problem demonstrates the need for additional specific constraints on the ferrous and ferric melt components under relevant redox conditions. This paper provides new measurement of the activities of liquid FeO^{liq} and $Fe_2O_3^{liq}$ in SiO_2-rich melt, in the presence of significant amounts of Fe^{3+} and under both anhydrous and hydrous conditions.

2. Background and previous work

Activities of FeO in a wide range of silicate melt compositions (a_{FeO}^{liq}) have been determined by geoscientists and material scientists (ref. in Table 1). The different approaches are summarized in Table 1. In most studies, activities of FeO^{liq} were determined by equilibrating pure metallic iron with a silicate melt at 1 atm with fO_2 slightly below the iron-wustite (IW) buffer. Under these conditions, iron is present in the melt almost solely as Fe^{2+}. The corresponding equilibrium may be written as:

$$Fe + \tfrac{1}{2} O_2 \Leftrightarrow FeO$$

metal gas melt

Table 1. Summary of previous determinations of activities of iron oxides in silicate melts.

Reference	Method	Standard state for the liquid	Thermodynamic data for the liquid	Equilibria	ΔG° (1 bar,J/mol)*
			Ferrous iron oxide component		
Schumann and Ensio (1951), Bodsworth (1959) Roeder (1974)	Pure Fe-metal equilibration	Unspecified	Unspecified	$Fe + ½\ O_2 \Leftrightarrow FeO^{liq}$	−230585 + 44.72. T
Doyle and Naldrett (1986)	Pure Fe-metal equilibration	Wustite liquid	Stull and Prophet (1971)	$Fe + ½\ O_2 \Leftrightarrow FeO^{liq}$	−247450 + 49.24. T
Doyle (1988; 1989)	Pure Fe-metal equilibration	Wustite liquid	Coughlin (1954)	$Fe + ½\ O_2 \Leftrightarrow FeO^{liq}$	−238771 + 48.53. T
Holzheid et al. (1997)	Fe-Ni-Co alloy equilibration	Wustite liquid	Barin (1989)	$Fe + ½\ O_2 \Leftrightarrow FeO^{liq}$	−244118 + 115.56. T − 8.474. T. ln T
Snyder and Carmichael (1991)	Fe-Ni alloy equilibration	Wustite solid	Coughlin (1954)	$0.947Fe + ½\ O_2 \Leftrightarrow Fe_{0.947}O^{sol}$	−265020 + 64.8. T
Matsuzaki et al (1998)	Pure Fe-metal equilibration	Wustite liquid	Banya et al. (1980)	$Fe + ½\ O_2 \Leftrightarrow FeO^{liq}$	−215853 + 35.65. T
		FeO liquid	Calculated from their study	$Fe + ½\ O_2 \Leftrightarrow FeO^{liq}$	−224393 + 42.79. T
O'Neill and Eggins (2002)	Pure Fe-metal equilibration	Wustite liquid	Barin (1989)	$Fe + ½\ O_2 \Leftrightarrow FeO^{liq}$	−244118 + 115.56. T − 8.474. T. ln T
This study	Fe-Ir alloy equilibration	FeO liquid	See appendix	$Fe + ½\ O_2 \Leftrightarrow FeO^{liq}$	−226244 + 42.49. T
This study	Hematite equilibration	FeO liquid	See appendix	$Fe_2O_3^{sol} \Leftrightarrow 2\ FeO^{liq} + ½\ O_2$	998615−342.43.T
			Ferric iron oxide component		
Snyder and Carmichael (1991)	Fe-Ni alloy equilibration	Hematite solid	Robie et al. (1978)	$Fe + ⅔\ O_2 \Leftrightarrow Fe_2O_3^{sol}$	−806222 + 248.65. T
This study	Fe-Ir alloy equilibration	Fe_2O_3 liquid	This study	$Fe + ⅔\ O_2 \Leftrightarrow Fe_2O_3^{liq}$	$-0.0562.\ T^2+374.59.\ T-846564$
This study	Hematite equilibration	Fe_2O_3 liquid	This study	$Fe_2O_3^{sol} \Leftrightarrow Fe_2O_3^{liq}$	$-0.0562.\ T^2+128.59.\ T-38275$

* Gibbs free energy of formation of the iron oxide melt component

Application of the law of mass action yields:

$$a_{FeO}^{liq} = \exp(\Delta G^{o}_{(1)}/RT)\, a_{Fe}\, (fO_2)^{1/2}$$

where a_{FeO}^{liq} is the activity of FeO in the melt, a_{Fe} is the activity of iron in metal, $\Delta G°_{(1)}$ is the Gibbs free energy change associated with equilibrium (1), R is the gas constant and T the temperature (see Table 1). Note that, at 1 bar, $\Delta G°(1)$ is simply the Gibbs free energy of formation of the ferrous iron oxide component in the melt, i.e., FeO in Eqn. 1. From Eqn. 2, at equilibrium between melt and pure Fe metal (i.e., $a_{Fe}^{metal} = 1$), the activity of FeO^{liq} is known if fO_2 and temperature are fixed. Curves of constant a_{FeO}^{liq} in a silicate melt equilibrated with pure Fe metal are shown on a T-log fO_2 plot (Fig. 1, see note on Fig. caption). The a_{FeO}^{liq} - X_{FeO}^{liq} relations have been determined with this approach for mafic to intermediate ferric iron-free melts at 1 bar and under anhydrous conditions [Roeder, 1974, Doyle and Naldrett, 1986, Doyle, 1988 and Doyle, 1989]. In the concentration range 0 to 17–18 wt.% FeO, activities of FeO^{liq} were found to follow Henry's law, with the Henry's constant a function of melt composition.

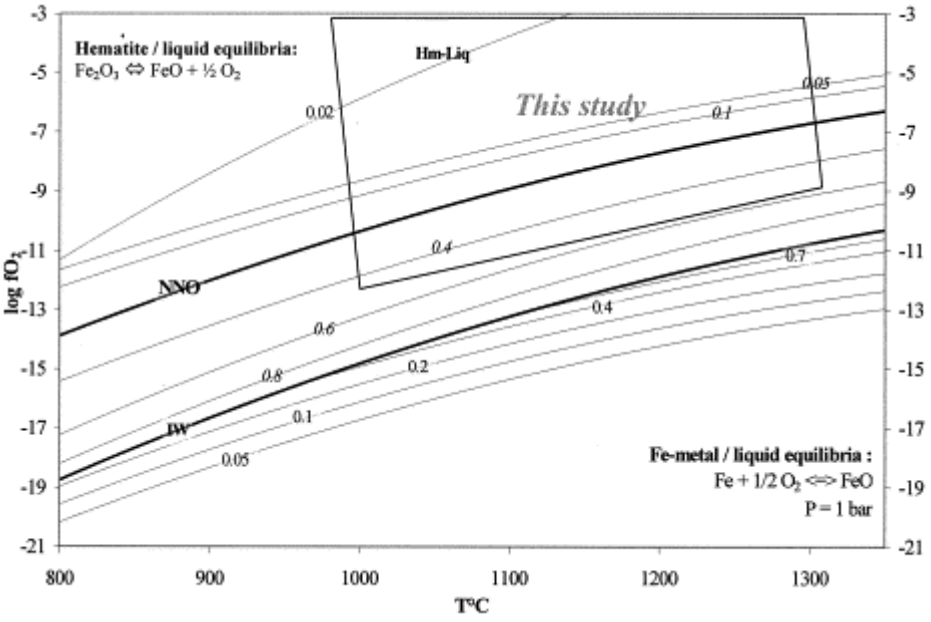

Fig. 1. T-fO_2 field of application of metal-liquid and hematite-liquid equilibria. The two bold curves are NNO (upper) and IW (lower) redox buffer calculated after Robie (1979). The black full lines below the IW buffer (lower part of the graph) are iso-a_{FeO}^{liq} lines defined by the pure Fe-silicate melt equilibrium calculated using eq. (3). Above the IW redox buffer, the dashed lines defined the T-fO_2 equilibrium between Fe-Ir alloys with different $X_{Fe}^{Ir\text{-}Fe}$ (values labeled on curves, calculated after Schwartzendruber, 1984) and silicate melts saturated with respect to pure magnetite (Ghiorso and Sack, 1991). The numbers shown on the dashed curves therefore represent the maximum of Fe that can be found in a Fe-Ir alloy in equilibrium with a silicate melts under the corresponding T-fO_2 conditions. Note the decrease of iron content in Fe-Ir alloys as fO_2 increases. In the upper part of the graph, a curve labeled Hm-Liq define the T-fO_2 domain of equilibrium between pure hematite and a silicate liquid with $a_{FeO}^{liq} = 0.02$ (calculated using eq. 9). The box indicates the T-fO_2 conditions explored in this study.

The pure Fe metal-silicate equilibration method is, however, limited to a T-fO_2 domain restricted to that below the iron-wustite buffer (Fig. 1), which corresponds to conditions much more reducing than most terrestrial magmas [Carmichael, 1991]. Two studies reported activities of FeO above IW and, consequently, in presence of significant amounts of ferric iron in the melt [Snyder and Carmichael, 1991 and Holzheid et al., 1997]. For these works, Fe^{3+} in the melt was not measured but calculated using the equation of [Snyder and Carmichael, 1991]. To extend the T-fO_2 field of application of the metal-silicate equilibration method, iron-bearing metallic alloys were used instead of pure Fe. Alloying of iron with other metallic elements decreases a_{Fe}^{metal} and thus shifts metal-silicate equilibrium to conditions more oxidizing than the IW buffer (Fig. 1). [Snyder and Carmichael, 1991] and [Holzheid et al., 1997] used, respectively, Fe-Ni and Fe-Ni-Co alloys to monitor $aFeO^{liq}$ in silicate melts at 1 atm for fO_2 up to $\sim$5 log units above the IW buffer. Although ferric iron is a minor component (Fe_2O_3 < 1 wt.%) under these conditions, the results of [Snyder and Carmichael, 1991] clearly show a positive dependence of the activity coefficient of FeO^{liq} (γ_{FeO}^{liq}) with the melt Fe^{3+}/Fe^{2+}. However, relatively few data points were obtained in the T-fO_2 field where Fe^{3+} is present as a major component. The a_{FeO}^{liq} database presently available (450 data points) is, therefore, still biased toward ferric iron-free compositions. [Snyder and Carmichael, 1991] also reported data on the activity of Fe_2O_3 in the liquid but the very low proportion of iron present as Fe_2O_3 (<10% of total Fe). The Fe_2O_3 content was estimated from the empirical regression of [Snyder and Carmichael, 1991] and not directly measured in the experimental glasses.

To complement and extend the available database on the activity of iron oxide components in silicate melts, we present below new a_{FeO}^{liq} and a_{Fe2O3}^{liq} data for SiO_2-rich melts, in presence of a significant proportion of ferric iron and for both anhydrous and hydrous conditions.

3. Experimental strategy

3.1. Principle

In this study, we have retained the principle of measuring a_{FeO}^{liq} and a_{Fe2O3}^{liq} under relatively oxidizing fO_2 conditions by equilibrating a Fe-bearing alloy with the silicate melt. Noble metal alloys (Fe-Ir) were preferred to the Fe-Ni alloys used in previous studies for several practical reasons. (1) Fe-Ir alloys are stable over a wide range of fO_2, being limited only by the Ir-IrO_2 equilibrium (log fO_2 $\sim$9 log units above NNO). In comparison, a_{FeO}^{liq} and a_{Fe2O3}^{liq} cannot be measured at fO_2 > NNO if Fe-Ni alloys are used (Fig. 1). (2) The Fe-Ir alloy (γgFe, Ir phase) forms a continuous solid solution from 0 to 100 at % Fe in the temperature range appropriate for equilibration with silicate melts, i.e., between $\sim$900°C and up to $\sim$1400°C [Massalski, 1992]. (3) Ir has very low solubilities in silicate melts, <100 ppb [Amossé and Alibert, 1993 and O'Neill et al., 1995] and the chemical properties of melts at equilibrium with metallic Ir are not expected to be significantly modified by the presence of dissolved Ir. (4) The mixing properties of the Fe-Ir alloy solid solution are known [Schwartzendruber, 1984] so that a_{Fe} can be calculated directly from X_{Fe}^{Fe-Ir}. [Woodland and O'Neill, 1997] confirmed the accuracy of the use of Fe-Ir alloys to calculate aFe at high-pressure high-temperature conditions by crosschecking equilibria involving Fe ± Ir, olivine and quartz. Despite these advantages, the Fe-Ir alloy-silicate equilibration method cannot be used above fO_2 imposed by the limit of detection of iron in the alloy (see Fig. 1). For the analytical conditions of this study (limit of detection of Fe of about 500 ppm, see below), this maximum fO_2 was found to be near NNO+2. Above this fO_2 value, a_{FeO}^{liq} and a_{Fe2O3}^{liq} were determined through the hematite-silicate instead of the Fe-Ir alloy-silicate equilibrium.

3.2. Standard states and calculation of activities

Previous determinations of activities of iron oxides in silicate melts have used various stoichiometries, standard states and thermodynamic data for the iron oxide melt components (Table 1). For the ferrous oxide component, a standard state of molten wustite ($Fe_{0.947}O$ liquid) has been commonly chosen despite the fact that molten wustite contains ≥ 13 wt.% Fe_2O_3 at fO_2 conditions corresponding to IW (see [Bowen and Schairer, 1934 and Schumann, 1951]. The difference in stoichiometry between FeO and molten wustite was accounted for by various means (for details see [Doyle and Naldrett, 1986, Doyle, 1988, Doyle, 1989, Holzheid et al., 1997 and O'Neill and Eggins, 2002]. [Snyder and Carmichael, 1991] adopted standard states of solid wustite and hematite, respectively, for the ferrous and ferric oxide components. To eliminate inconsistencies due to differences in standard states and/or thermodynamic data, and to allow comparison between studies, the same liquid standard states and thermodynamic data have been adopted, as detailed below, and activities from previous studies have been recalculated.

In this study, stoichiometric FeO and Fe_2O_3 liquids were chosen as melt components. Their standard states were calculated from the elements at temperature and pressure. Because thermodynamic data are available for neither component, their standard state properties needed to be estimated. The properties of liquid FeO were estimated from a thermodynamic analysis of the pseudobinary system SiO_2-FeO±Fe_2O_3 at 1 atm [Bowen and Schairer, 1934, Schumann, 1951 and Bodsworth, 1959]. The approach and method of numerical optimization are detailed in appendix of this paper. Results (Table 1; Fig. 2a) yield an expression for the Gibbs free energy of formation for liquid FeO at 1 bar, which is near that adopted in early and recent studies [Schumann, 1951, Bodsworth, 1959 and Matsuzaki et al., 1998]. The activity of liquid FeO is then calculated from equilibrium (1) and Eqn. 2 at known P, T, fO_2 and a_{Fe} (from X_{Fe}^{metal}). The molar volumes of FeO liquid and Fe metal were taken respectively from [Lange and Carmichael, 1990] and [Woodland and O'Neill, 1997]. This yields the following expression for a_{FeO}^{liq}:

$$a_{FeO}^{liq} = a_{Fe}\,(fO_2)^{1/2} \exp\left((-226244 + 42.49T + P.\,(0.483 + 8.633.\,10^{-}5T - 3.784.10^{-6}P))/RT\right)$$

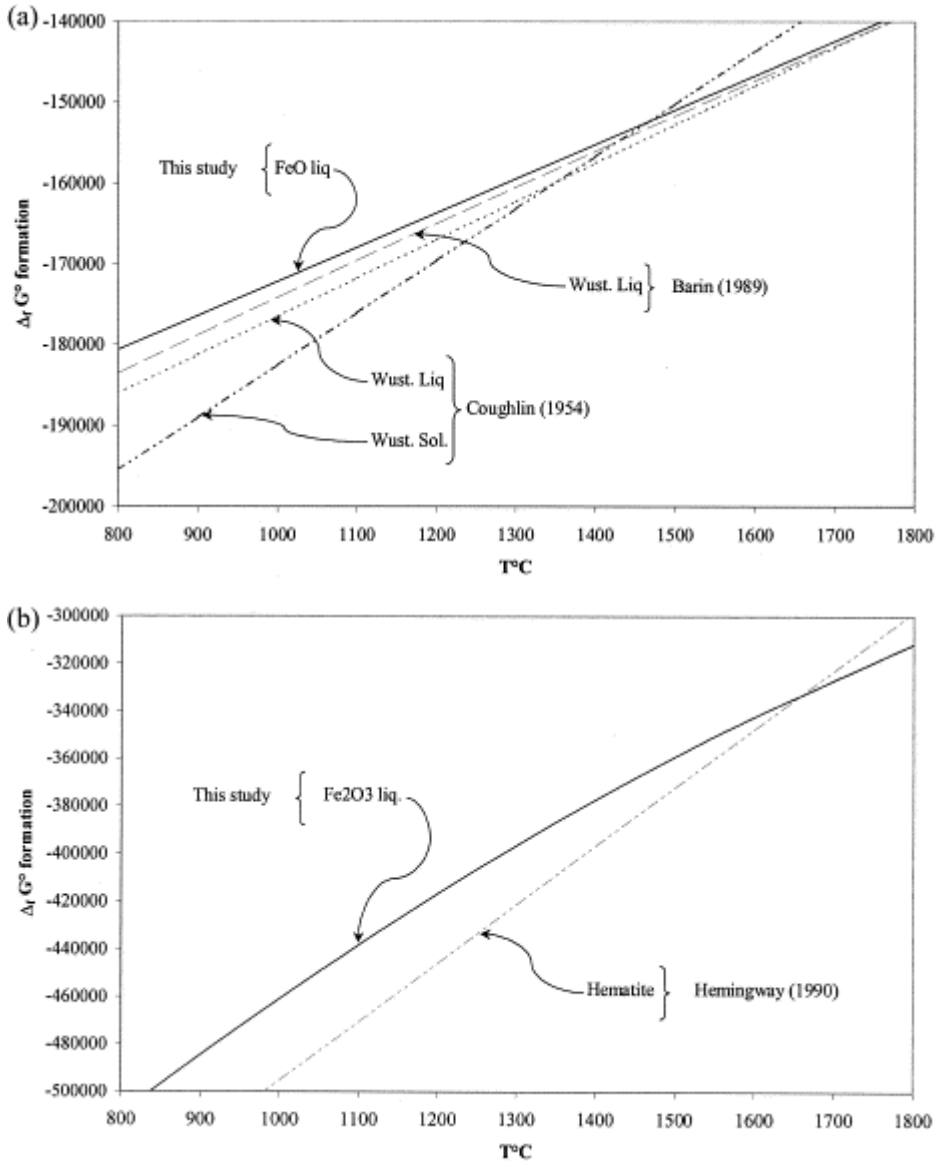

Fig. 2. (A) Gibbs free energy of formation from the elements at P and T of liquid FeO, liquid wustite and solid wustite. (P = 1 bar). For details of source data see Table 1. (B) Gibbs free energy of formation from the elements at P and T of liquid Fe_2O_3 and solid Hematite. (P = 1 bar). For details of source data see Table 1.

For liquid Fe_2O_3, we have taken the entropy of melting of hematite estimated by [Ghiorso and Sack, 1995]. From the melting point and the standard state thermodynamic properties of hematite [Ghiorso and Sack, 1991], together with Cp_{Fe2O3}^{liq} [Lange and Navrotsky, 1992], the thermodynamic properties of liquid Fe_2O_3 were calculated at any temperature (Fig. 2b; Table 1). The activity of Fe_2O_3 is then calculated from the equilibrium:

$$2Fe + 3/2O_2 \Leftrightarrow Fe_2O_3$$

metal gas meltwhere:

$$a_{Fe2O3}^{liq} = a_{Fe}^{2} (fO_2)^{1.5} \exp(\Delta G°_{(5)}/RT)$$

at known P, T, fO_2 and a_{Fe} (from X_{Fe}^{metal}). $\Delta G°(5)$ is taken from Table 1. The molar volumes of liquid Fe_2O_3 and Fe metal are taken respectively from [Lange and Carmichael, 1990] and [Woodland and O'Neill, 1997]. The following expression for a_{Fe2O3}^{liq} is then obtained:

$$a_{Fe2O3}^{liq} = a_{Fe}^{2} (fO_2)^{1.5} \exp((-0.0562\ T^2 + 374.59\ T - 846564 + P\ (1.334 + 0.8.10^{-4}\ T - 0.24510^{-4}\ P))/RT)$$

We ignore any volume dependence of Fe_2O_3 on the melt composition or structural positions of Fe_2O_3 because no data exists and, in the pressure range of this study, the volume effect on the calculated activity should negligibly affect the activities.

For experiments conducted above NNO+2, activities where obtained via the hematite-liquid equilibria (see above and Fig. 1):

$$Fe_2O_3 \Leftrightarrow 2FeO + \tfrac{1}{2} O_2$$

hematite liquid gasand:

$$Fe_2O_3 \Leftrightarrow Fe_2O_3$$

hematite liquid

The a_{FeO}^{liq} and a_{Fe2O3}^{liq} are calculated from data in Table 1 and [Lange and Carmichael, 1990] for the melt components, and from [Ghiorso and Sack, 1991] for hematite (standard state properties, volume, activity-composition relations). This yields the following expressions:

$$a_{FeO}^{liq} = a_{Fe2O3}^{Hm}\ fO_2^{1/2} \exp((-342.43\ T + 998615 + P\ (-1.242 + 0.00046\ T - 7.537.10^{-6}\ P))/RT)$$

$$a_{Fe2O3}^{liq} = a_{Fe2O3}^{Hm} \exp((-0.0562\ T^2 + 128.59\ T - 38275 + P\ (-0.3027 + 0.00079\ T - 2.284\ 10^{-5}\ P)/RT)$$

where a_{Fe2O3}^{Hm} is the activity of Fe_2O_3 in hematite.

Uncertainties on a_{FeO}^{liq} and a_{Fe2O3}^{liq} were estimated by propagating the uncertainties in T ($\sim$ 10–15°C), X_{Fe}^{metal} (5 to 15%), $\gamma_{Fe}^{Ir\text{-}Fe}$ (see [Woodland and O'Neill, 1997], and fO_2 (0.05–0.3 log unit). For hydrothermal experiments, fO_2 uncertainties are due to uncertainty in the sensor method calibration and uncertainty in f_{H2O} in the melt (see hereafter). For 1 atm experiments, a crosschecking between fO_2 given by the zircon probe and fO_2 estimated from the gas flow indicates maximum departures of $\sim$0.05 log units. The mean uncertainties on a_{FeO}^{liq} and a_{Fe2O3}^{liq} are about 10% but can reach 18% for alloys with low X_{Fe}^{alloy} and 25% for the water-undersaturated experiments, which have the largest uncertainties on fO_2.

4. Experimental and analytical techniques

4.1. Starting materials

Compositions of the 15 starting glasses are listed in Table 2. They have SiO_2 contents ranging between ~69 and ~78 wt.% and FeO_{tot} between ~0.5 and ~9 wt.%. The first series of glasses is calcium-free with several compositions (# 2, 4, 6, 8, 9) used previously to determine the effect of H_2O and fO_2 on the ferric-ferrous ratio of silicic melts [Gaillard et al., 2001]. A second series of glasses contains different proportion of calcium. All glasses have nearly identical Si_4O_8 contents (between 56 and 63 mol.%, see below for a definition of the melt components). Within the series of calcium-free glasses, FeO_{tot} contents vary at constant $KAlO_2/NaAlO_2$. The calcic glasses have constant FeO_{tot} contents and $KAlO_2/NaAlO_2$, with CaO substituting for the alkali in equal molar proportions. Some glasses are slightly peraluminous and the others slightly peralkaline. Therefore, apart from the Ca = Na + K substitution and the small deviations from the metaluminous plane, the starting glasses can be viewed as pseudobinary mixtures between an aluminosilicate component of nearly constant composition and FeO_{tot}. All glasses were obtained from gels prepared with the method of [Pichavant, 1987], melted at ~1400 °C in air and then quenched. In most experiments, small amounts of iron were added (as Fe metal and/or Fe_2O_3) to compensate for the loss of iron to the sample containers and Ir alloys (Table 3). Mixtures of silicate glass and Fe/Fe_2O_3 were homogenized and then ground in an agate mortar. The amount of iron added to the silicate base was estimated from [Gaillard et al., 2001] for runs conducted in gold capsule, from [Kawamoto and Hirose, 1994] for runs with Au-Pd container and from [Toplis and Carroll, 1996] for Pt capsule.

Table 2. Starting compositions

#	1	2	3	4	5	6	7	8	9	10	11	12	Ca1	Ca2	Ca3
SiO_2	75.84	78.33	75.77	77.17	75.57	77.08	75.66	76.77	76.2	73.44	70.45	69.29	76.32	74.17	76.33
Al_2O_3	11.93	11.77	12.31	12.07	12.64	11.79	11.92	11.45	11.50	11.11	12.26	11.70	11.96	13.29	11.92
FeO*	0.56	0.83	1.08	1.55	1.85	2.58	2.86	3.38	4.25	6.07	7.32	9.28	2.08	2.39	1.97
CaO	0.01	0.03	0.00	0.01	0.01	0.02	0.03	0.04	0.03	0.03	0.00	0.02	0.86	1.87	2.51
Na_2O	4.07	4.05	4.24	4.02	3.84	3.74	3.50	3.71	3.67	3.00	3.45	3.16	3.22	2.99	2.40
K_2O	5.46	4.97	5.34	4.72	4.97	4.76	4.84	4.67	4.36	4.05	4.60	4.20	4.27	3.73	2.81
Total**	97.88	99.90	98.75	99.85	98.88	99.90	98.79	99.98	100.06	97.71	98.08	97.65	98.72	98.45	97.95
A1/CNK***	0.95	0.98	0.97	1.06	1.08	1.04	1.08	1.03	1.07	1.19	1.15	1.20	1.04	1.08	1.03

* FeO total analyzed on EMPA is reported.
** Original total on EMPA.
*** $Al_2O_3/(CaO + Na_2O + K_2O)$ in mole.

Table 3. Test of Pt-Ir interaction: Runs performed at 1380°C, QFM, 1 atm, 10 days.

	Starting composition	Run products (EMPA)			
	Glass (wt %)	Glass* (wt %)	Fe-Ir powders**	Fe-Pt wire***	Ternary Fe-Ir-Pt****
SiO_2	49.58	51.1 (73)			
Al_2O_3	17.74	18.02 (32)			
FeO	8.04	4.80 (20)			
MgO	5.39	5.90 (21)			
CaO	10.61	11.90 (31)			
Na_2O	4.28	3.20 (15)			
TiO_2	1.32	1.41 (23)			
Cr_2O_3	0.01	0.01 (2)			
K_2O	2.12	2.57 (12)			
Total	99.09	98.82 (79)			
Nb. points	14	18	23	8	1
X_{Fe}			0.063 (0.002)	0.185 (0.003)	0.12
X_{Ir}			0.935 (0.004)	0	0.55
X_{Pt}			0	0.815 (0.003)	0.33
a_{FeO}			0.081 (0.007)	0.077 (0.005)	?

* Crystal-free glass analyzed after experiments. The two-sigma in brackets applies to the last number after the coma. The two-sigma value for FeO_{tot} equal +/− 0.20 wt% demonstrates the homogeneity iron content in the melt and thus attainment of equilibrium of iron partitioning between liquid and metal.

** Pure Fe-Ir alloys analyzed: The composition of these grains represents about 90% of the accessible grains.

*** Pure Fe-Pt alloys analyzed: The composition of these alloys represents about 80% of the Pt-wire.

**** Example of an alloy Fe-Ir-Pt. The zone were these ternary alloys were founded was about 50μm around the Pt-wire.

For experiments at 1 atm, about 1 wt.% of pure iridium powder (grain size ~10 μmm) was added to and homogeneously mixed with the silicate glass ± Fe/Fe_2O_3 powder. Iridium-free mixtures were also prepared and run in parallel with the iridium-bearing mixtures, the resulting glasses being used for the analysis of FeO and the determination Fe^{3+}/Fe^{2+} of the glass. Starting products were suspended on Pt wires (sample/Pt mass ratio ~10) and subsequently placed in the hot spot of a 1 atm gas-mixing furnace.

For experiments at 2 kbar, wires of iridium metal (diameter 75 μm, see Fig. 3) were initially used as the source of Ir. This method resulted in impracticably long experimental durations (i.e., ≥25 d), mainly because of the slow kinetics of diffusion of Fe in Ir metal. To decrease the duration necessary for attainment of equilibrium, iridium was later introduced as in the 1 atm experiments, i.e., as powders of ~10 μm grain size premixed with the silicate glass ± Fe and/or Fe_2O_3 (Fig. 3). As for 1 atm, iridium-free starting silicate glass ± Fe and/or Fe_2O_3 mixtures were run in parallel with the iridium-bearing mixtures. The starting products were loaded in noble metal capsules together with known quantities of distilled water. A majority of experiments were performed under H_2O-saturated conditions. The charges typically consisted of ~10 mg of H_2O for ~100 mg of the solid materials. For the H_2O-undersaturated experiments, H_2O in the charges ranged between 2 and 10 mg. Either Au, Au-Pd or Pt capsules (length 15–20 mm, internal diameter 2.5 mm, wall thickness of either 0.1 or 0.2 mm) were used depending on the experimental temperature

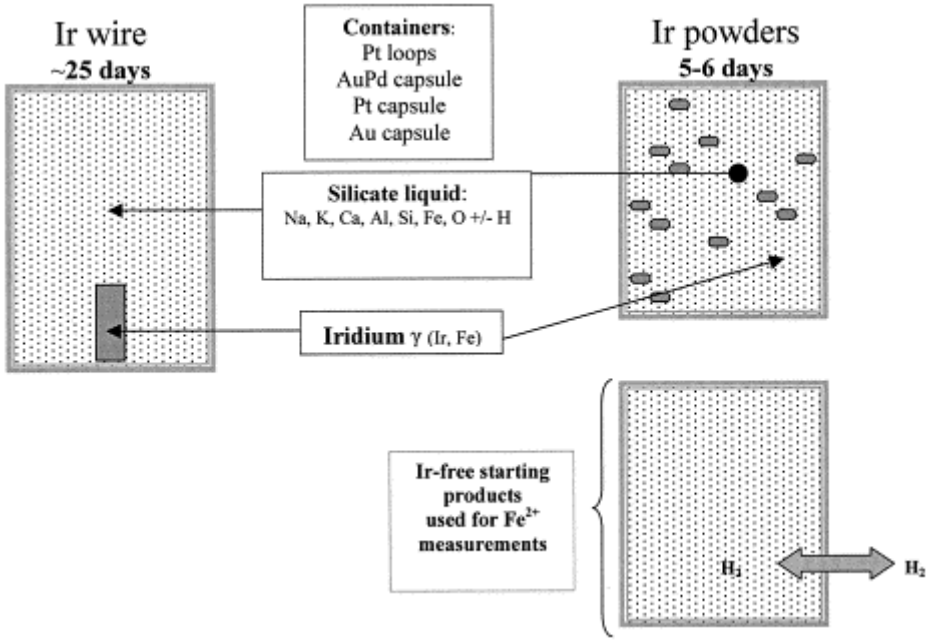

Fig. 3. Protocols used for Ir addition to the silicate base for 1 atm experiments and high-pressure runs.

Table 4. Experimental conditions and activity results.

# Run	# Sample	Starting products	Activity sensors	H_2O %wt	Δ NNO	a_{FeO}^{liq}	a_{Fe2O3}^{liq}
1210°C, 0.001 Kb, NNO-1.28, 25 days							
1	1/1	#3 + $_{Fe2O3}$	Ir powders/Pt wires	0	−1.28	0.157/0.147	0.0009/0.0011
	1/2	#3 + $_{Fe2O3}$	Pt wire	″	″	0.159	0.0011
	1/3	#3 + *Fe*	Ir powders/Pt wires Pt	″	″	0.110/0.105	0.0004/0.0004
	1/4	#3 + $_{Fe2O3}$	wire	″	″	0.100	0.0013
	1/5	#3 + *Fe* + $_{Fe2O3}$	Ir powders/Pt wires	″	″	0.054/0.057	0.0001/0.0001
	1/6	#3 + $_{Fe2O3}$	Pt wire	″	″	0.057	0.0004
	1/7	#3 + *Fe*	Ir powders/Pt wires	″	″	0.029/0.027	0.00004/0.00002
	1/8	#3 + *Fe* + $_{Fe2O3}$	Pt wire	″	″	0.028	0.0001
1160°C, 2 Kb, fH_2^b = 105 bar, water saturated, 4 days							
2	2/1	#5 + *Fe* + Fe_2O_3	Ir powders	5.21	−1.25	0.106	0.0007
	2/2	#5 + *Fe* + Fe_2O_3	–	4.99	″	–	–
	2/3	#5 + *Fe* + Fe_2O_3	Ir powders	5.56	″	0.063	0.0003
	2/4	#5 + *Fe* + Fe_2O_3	–	5.61	″	–	–
	2/5	#5 + *Fe* + Fe_2O_3	Ir powders	4.96	″	0.119	0.0009
	2/6	#5 + Fe_2O_3	–	5.30	″	–	–
	2/7	#5 + Fe_2O_3	Ir powders/Pt capsule	5.03	″	0.028/0.032	0.00005/0.00006
	2/8	#5 + *Fe* + Fe_2O_3	Pt capsule	5.00	″	0.051	0.0002
1000°C, 2 Kb, $fH2^b$ = 125 bar, 6 days							
3	3/1	#5 + *Fe* + $_{Fe2O3}$	Ir Powders	3.03	−2.85	0.064	0.00007
	3/2	#5 + *Fe*	″	5.55	−1.91	0.015	0.00001
	3/3	#5 + *Fe*	″	5.96	−1.91	0.107	0.0006
	3/4	#7 + *Fe* + $_{Fe2O3}$	″	5.40	−2.08	0.109	0.0005
	3/5	#7 + *Fe* + $_{Fe2O3}$	″	3.41	−2.66	0.076	0.0001
	3/6	#3 + *Fe* + $_{Fe2O3}$	″	6.28	−1.95	0.055	0.0001
	3/7	#5 + $_{Fe2O3}$	″	6.54	−1.91	0.042	0.00009
	3/8	#3 + $_{Fe2O3}$	″	5.15	−2.18	0.011	0.00000
	3/9	#3 + *Fe*	″	4.16	−2.39	0.104	0.0003
	3/10	#5 + *Fe* + $_{Fe2O3}$	″	6.65	−1.91	0.030	0.00005
	3/11	#5 + *Fe*	″	2.40	−3.16	0.028	0.00001
	3/12	#5 + *Fe* + $_{Fe2O3}$	″	6.00	−1.91	0.048	0.0001
	3/13	#5 + *Fe* + *Fe*	″	5.94	−1.91	0.050	0.0001
1000°C, 2 Kb, $fH2^b$ = 31 bar, water saturated, 16 days							
4	4/1	#2	Ir Wire	5.12	−0.8	0.011	0.00002
	4/2	#3	″	5.95	−0.8	0.018	0.00005
	4/3	#4	″	5.24	″	0.025	0.0001
	4/4	#5	″	5.32	″	0.041	0.0003
	4/5	#8	″	5.26	″	0.063	0.0007
	4/6	#10	″	5.07	″	0.085	0.0021
	4/7	#11	″	4.49	″	0.112	0.0035
	4/8	#12	″	4.50	″	0.120	0.0040
1000°C, 2 Kb, $fH2^b$ = 22 bar, water saturated, 6 days							
5	5/1	#11	Ir Wire	5.10	−0.5	0.159	0.0055
	5/2	#12	″	4.50	″	0.188	0.0087
1000°C, 2 Kb, fH2 = 2.4 bar, water saturated, 6 days							
6	6/1	#1	Ir Powders	~6.68	+1.4	0.012	0.0002
	6/2	#2	″	~6.97	″	0.030	0.0015
	6/3	#5	″	~6.58	″	0.059	0.0056
	6/4	#6	″	~6.97	″	0.076	0.0093
	6/5	#9	Ir powders/Magnetite	~7.15	″	0.092/0.087	0.0136/0.01300
	6/6	#10	Ir powders/Magnetite	~6.80	″	0.085/0.080	0.0118/0.0109
	6/7	#1	–	5.54	″	–	–
	6/8	#2	–	5.43	″	–	–
	6/9	#5	–	5.26	″	–	–
	6/10	#6	–	5.23	″	–	–
	6/11	#9	Magnetite	~6.45	″	0.090	0.0132
	6/12	#10	Magnetite	~6.81	″	0.084	0.0110
1245°C, 0.001 Kb, air, 25 days							
7	7/1	#Ca3 + *Fe* + Fe_2O_3	Hm	0	+7.3	0.017	0.099
	7/2	#Ca2 + Fe_2O_3	″	″	″	0.017	0.102
	7/3	#Ca1 + *Fe* + Fe_2O_3	″	″	″	0.017	0.102
	7/4	#3 + *Fe*	″	″	″	0.017	0.096

4.2. Experimental techniques

Experiments were conducted at both 1 atm and 2 kbar. For the 1 atm experiments, a vertical SiC resistance furnace was used. Temperature was monitored by a type S thermocouple and is known to within ± 5 °C. CO_2-CO gas mixtures with proportions calculated from [Deines et al., 1974] served to impose the experimental fO_2 which was measured directly by an yttria-stabilized zirconia probe with an uncertainty of 0.02–0.05 log unit (see above). A drop quench technique was used at the end of the experiments. The 2 kbar experiments were performed in an internally heated pressure vessel fitted with a rapid quench device modified after [Roux and Lefèvre, 1992]. A two-windings furnace adapted from the device of [Roux et al., 1994] was used. Temperature was measured by three type B thermocouples with estimated uncertainties (including thermal gradients) of ± 10°C at 1000°C and ± 15°C at the highest temperature investigated (1160°C). Pressure was imposed by Ar-H_2 mixtures, whose fH_2 served to control the redox conditions through the equilibrium:

$$H_2 + \tfrac{1}{2} O_2 \Leftrightarrow H_2O$$

which shows that fO_2 is fixed if fH_2 is imposed to a H_2O-bearing system of known fH_2O [Scaillet et al., 1992 and Scaillet et al., 1995]. The fH_2 was not constantly monitored using a Shaw membrane but it was determined for each run using the Co-Ni-Pd redox sensors [Taylor et al., 1992 and Pownceby and O'Neill, 1994]. The fO_2 was subsequently calculated with fH_2O either taken from [Burnham et al., 1969] for the water-saturated experiments, or computed from glass H_2O contents and the model of [Silver et al., 1989] for the water-undersaturated experiments. Uncertainties in fO_2 were propagated through uncertainties in fH_2 calculated from redox sensor (1–5% depending on fH_2 value) and uncertainties in f_{H2O} of the melt (10%). At water saturation, fO_2 are shown to be accurate to within 0.1 log units and for water-undersaturated conditions, uncertainties rose to 0.3 log units.

4.3. Analytical methods

Experimental products, including glasses, oxide minerals, and Fe-Ir alloys, were analyzed with a Cameca SX-50 electron microprobe of the BRGM-CNRS laboratories at Orléans, France. Silicate glasses and oxide minerals were analyzed under the following operating conditions: acceleration voltage 15 kV, sample current 6 nA, counting time on peak 10 s. A beam size of 1–2 μm was employed for oxide minerals whereas, for glass analysis, the beam was defocused to $\sim$10 μm to minimize the migration of alkali [Pichavant, 1987]. The H_2O content of experimental glasses was estimated from the by-difference method [Devine et al., 1995], calibrated against a set of internal hydrous glass standards analyzed together with the unknowns during each microprobe session. Results were cross-checked with FTIR determinations on selected samples (see below and [Gaillard et al., 2001]. Fe-Ir alloys were analyzed under an acceleration voltage of 20 kV, a sample current of 20 nA, with counting times of 20 and 10 s on peak and background respectively and an electron beam focused to 1–2 μm. Standards were pure metal Fe and Ir. Several other elements (S, Au, Pt, Pd, Si and Ni) were systematically analyzed together with Fe and Ir. Due to the small size ($\leq\sim$10 μm) and porous texture of the Fe-Ir alloys, their analysis was difficult and the data indicated contamination with glass, more rarely magnetite. To overcome this problem, analyses were

replicated until a minimum of 6–7 satisfactory analyses were obtained per sample, with the Si and Ir concentrations being taken as indicators of the extent of glass contamination. Under our analytical conditions, the limit of detection of Fe in the alloy is about 500 ppm.

A wet chemical technique, based on potassium dichromate titration, was used to measure the ferrous iron content (i.e., FeO) of glasses [Thornber et al., 1980 and Gaillard et al., 2001]. Details of the method and tests of reproducibility and accuracy were provided by [Gaillard et al., 2001]. The analytical uncertainty (expressed in wt.% FeO) increases with FeO, i.e., ± 0.02 at 0.3 wt.% FeO and ± 0.15 at 7 wt.% FeO. The Fe_2O_3 content of glasses was calculated by difference between total iron analyzed by electron microprobe (EMPA) and ferrous iron following:

$$Fe_2O_3 \text{ wt\%} = (FeO_{tot} - FeO)\ 1.1113$$

Only glasses from experiments performed with Ir-free starting mixtures were analyzed. The relationships between ferrous and total iron content were then established and fitted for Ir-free samples synthesized during each run (see results, 5.2.1, 5.2.2). These empirical relationships were used to calculate the FeO (and Fe_2O_3) contents of Ir-bearing glasses whose total iron contents were known from EMPA. Some glasses were not totally crystal-free, containing small amounts of either magnetite or hematite (see results). These Fe-oxides were shown to be in equilibrium with the melt and therefore, they should not be quenched phases (see results, 5.1.2). For these oxide-bearing samples, the FeO content of the glass was obtained by the empirical fit relating ferrous to total iron of the melt calibrated on crystal free samples. The ferric iron content in the glass was calculated from the measured total iron and calculated ferrous iron in the glass. This method was preferred to mass balance calculations that would consist in subtracting the contribution of oxides to the ferric-ferrous ratio of the sample to estimate the glass Fe^{3+}/Fe^{2+}. This mass balance method was shown to propagate significant uncertainties in some case (see [Gaillard et al., 2001] for details).

For selected samples, infrared spectrometry was used to determine the glass OH and H_2O contents. Doubly polished glass wafers with known thickness were placed under the beam of a Nicolet 760 Magna FTIR spectrometer. Analytical procedures were the same as described by [Gaillard et al., 2001]. Extinction coefficients from Newman et al. (1986) were used to calculate the OH and H_2O content (wt.%) from peak heights of the absorption bands at $4500cm^{-1}$ and $5200cm^{-1}$ respectively. Because fluid inclusions, Fe oxide minerals and/or metallic powders may be present locally, glass densities were not measured but calculated with the same methods as in [Gaillard et al., 2001]. The calculated density agrees within less than 10% with recent density measurements for glasses of similar compositions [Behrens and Jantos, 2001].

5. Results

5.1. Equilibrium and internal consistency

Determination of a_{FeO}^{liq} and a_{Fe2O3}^{liq} requires attainment of chemical equilibrium, either between Fe-Ir alloy and melt for fO_2 < NNO+2 (equilibria (1) and (5)) or between hematite and melt above NNO+2 (equilibria (8), (9)). Attainment of equilibrium was tested by performing time-series experiments. The activity determinations were cross-checked with

independent equilibria, involving either noble metals others than Ir or magnetite. Strictly speaking, no reversals were performed (i.e., compositions of alloys were not reversed by duplicating experiments starting with pure Ir with others performed for example with $Fe_{50}Ir_{50}$ alloys). However, Fe metal was present in most starting mixtures (Table 4) and alloy compositions were thus approached from both sides (i.e., pure Fe and pure Ir). Chemical equilibrium for the metallic iron and iron oxide components was demonstrated by using the following criteria: (1) attainment of homogeneous chemical compositions for glasses, for Fe-Ir alloys and for noble metal suspension wires/containers, (2) internal consistency of a_{Fe}, a_{FeO}^{liq} and a_{Fe2O3}^{liq} calculated from independent equilibria, which is the basic definition of thermodynamic equilibrium (equality of chemical potentials). These different lines of evidence are detailed below.

5.1.1. 1 atm experiments

At $\sim$1200°C, several weeks were needed for attainment of equilibrium. The main problem encountered is the loss of iron to the Pt suspension wire. This causes iron depletion in the melt near the wire and produces heterogeneity in FeO_{tot} of glasses. At 1210°C, experiments of 25 d (run 1, Table 4) were required to obtain glasses with homogeneous FeO_{tot} (Fig. 4a, b). Once the melt iron content is homogeneous, the analyzed Fe-Ir alloys are also homogeneous (Fig. 4c), suggesting that the kinetics of equilibration between Fe-Ir alloy and melt is faster than the kinetics of Fe equilibration with Pt loops by diffusion in the anhydrous melt (see also [Woodland and O'Neill, 1997]. However, to ensure that equilibrium was reached, each 1-atm run was performed for durations of 25 d. At constant fO_2, the Fe^{3+}/Fe^{2+} of glasses synthesized from starting products with different proportions of metal Fe and Fe_2O_3 are close to each other (see Table 4 and Table 5, runs # 1, 7, 8), suggesting that the iron redox equilibrium is attained or closely approached. In run # 1 (Table 4), compositions of the Pt-Fe suspension wires (Fig. 4b) served to crosscheck the activity calculation from Ir-Fe [Heald, 1967 and Schwartzendruber, 1984]. Results show that a_{Fe}^{metal} (and hence μ_{Fe}^{metal}) are identical within error in both alloys (Fig. 5), the two activity sensors yielding nearly identical a_{FeO}^{liq} and a_{Fe2O3}^{liq} (Table 4). Because the Pt wire and the Ir powders are not in direct contact but are separated by the melt, the identity in μ_{Fe}^{metal} implies that each alloy is in equilibrium with the silicate melt (equilibria (1), (5)). For runs # 7 and 8, performed in air, hematite-liquid equilibria could not be crosschecked with metal-liquid equilibria because the Fe concentration in the alloys is below detection under these fO_2 conditions. However, a_{FeO}^{liq} and a_{Fe2O3}^{liq} are similar in runs performed with starting materials having different proportions of metal Fe and Fe_2O_3 (Table 4). This is interpreted as evidence for attainment of equilibrium in these two runs.

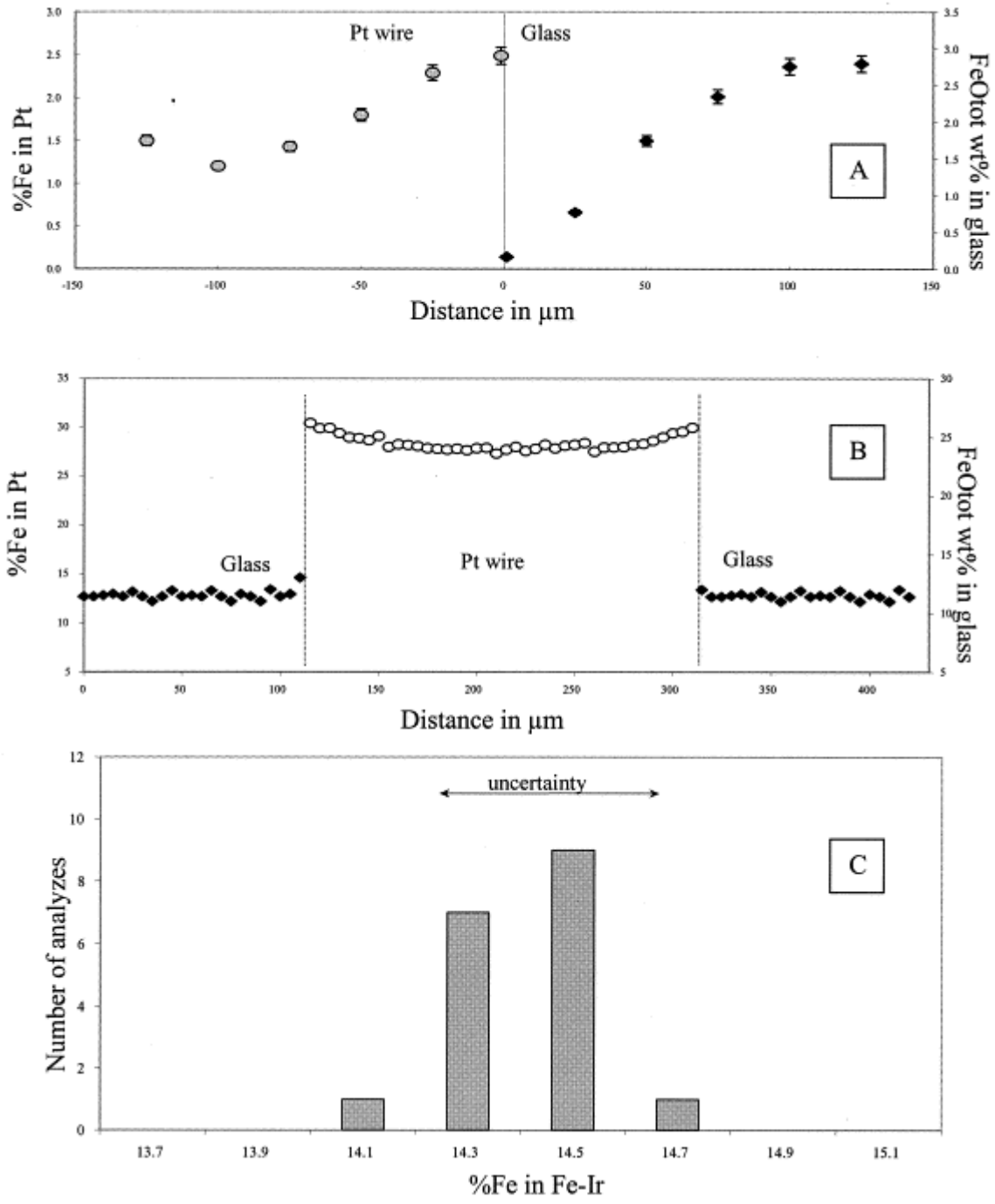

Fig. 4. Melt-Pt-Ir equilibria at one atm. (A): Non-equilibrated profile at the melt-Pt boundary (10 days, non tabulated); (B, C): Equilibrated, 25 days, (see Table 4 and Table 5): (B) Profile in the Pt wire and at the melt-Pt boundary in sample #1/2. (C) Histogram of Fe content in 18 analysed Fe-Ir grains of the sample #1/3.

Table 5. Chemical composition of phases. (See for activities calculated from alloys and/or oxides composition and fO_2).

Methods	EMPA									FTIR		Wet Chemistry		
Phases	Glasses or Oxides when specified							Alloys		Glasses				
# Sample	SiO_2	Al_2O_3	FeO	CaO	Na_2O	K_2O	H_2O	X $Fe^{(Ir)}$	X $Fe^{(Pt)}$	OH/H_2O	H_2O	FeO wt%	Fe_2O_3	X Fe_2O_3/XFeO
1210°C, 0.001 Kb, NNO-1.28, 25 days														
1/1	69.08	11.75	10.37	0.00	3.11	4.23	–	0.17	0.30	n.d.	n.d.	9.55	0.91	0.04
1/2	68.14	11.50	11.85	0.07	3.08	4.28	–		0.31	n.d.	n.d.	10.37	1.65	0.07
1/3	71.96	11.75	7.35	0.08	3.35	4.55	–	0.14	0.26	n.d.	n.d.	6.99	0.40	0.03
1/4	71.65	11.82	7.89	0.07	3.29	4.49	–		0.28	n.d.	n.d.	7.60	0.32	0.02
1/5	74.21	11.89	4.26	0.00	3.54	4.71	–	0.11	0.25	n.d.	n.d.	4.13	0.15	0.02
1/6	74.04	12.01	4.67	0.00	3.59	4.65	–		0.25	n.d.	n.d.	4.50	0.19	0.02
1/7	75.68	12.05	2.10	0.04	3.80	4.80	–	0.07	0.18	n.d.	n.d.	2.06	0.05	0.01
1/8	75.91	12.10	2.29	0.06	3.71	4.86	–		0.22	n.d.	n.d.	2.20	0.10	0.02
1160°C, 2 Kb, fH_2[b] = 105 bar, water saturated, 4 days														
2/1	66.79	10.38	8.84	0.02	3.05	4.43	5.21	0.15		n.d.	n.d.	7.18	1.84	0.12
2/2	65.30	10.22	10.64	0.01	3.25	4.35	4.99			n.d.	n.d.	8.40	2.49	0.13
2/3	69.94	10.95	4.27	0.02	3.32	4.58	5.56	0.12		n.d.	n.d.	3.80	0.52	0.06
2/4	69.22	10.72	5.23	0.01	3.27	4.59	5.61			n.d.	n.d.	4.50	0.81	0.08
2/5	65.95	10.34	9.85	0.05	3.20	4.39	4.96	0.16		n.d.	n.d.	8.01	2.05	0.12
2/6	65.74	10.25	9.81	0.04	3.17	4.40	5.30			n.d.	n.d.	8.00	2.01	0.11
2/7	72.89	11.32	1.78	0.03	3.34	4.78	5.03	0.07	0.16	n.d.	n.d.	1.62	0.18	0.05
2/8	72.08	11.16	3.55	0.01	3.35	4.77	5.00		0.18	n.d.	n.d.	3.15	0.44	0.06
1000°C, 2 Kb, $fH2^b$ = 125 bar, 6 days														
3/1	71.60	11.63	4.54	0.01	3.55	4.60	3.25	0.32		1.1/1.93	3.03			
3/2	71.67	11.76	0.82	0.01	3.52	4.47	6.71	0.11		1.38/4.17	5.55			
3/3	68.46	10.57	6.05	0.02	3.19	4.15	6.55	0.26		1.35/4.61	5.96			
3/4	68.00	10.64	7.15	0.01	3.13	4.15	5.85	0.28		1.28/4.12	5.40			
3/5	71.54	11.74	4.77	0.03	2.90	4.50	3.56	0.31		0.98/2.43	3.41			
3/6	70.38	10.62	3.27	0.02	3.56	4.21	6.59	0.21		1.37/4.91	6.28			
3/7	71.07	10.66	2.45	0.01	3.31	4.21	6.88	0.18		1.4/5.14	6.54			
3/8	72.88	11.72	0.70	0.03	3.69	4.44	6.02	0.11		1.37/3.78	5.15			
3/9	68.69	10.89	7.46	0.01	3.29	4.30	4.99	0.31		1.15/3.01	4.16			
3/10	71.70	10.72	1.69	0.02	3.43	4.11	7.1	0.16		1.42/5.23	6.65			
3/11	75.40	11.34	1.81	0.01	3.70	4.46	2.66	0.27		0.85/1.55	2.40			
3/12	71.32	10.67	2.63	0.01	3.60	4.19	6.44	0.19		1.45/4.55	6.00			
3/13	71.44	10.74	2.41	0.02	3.67	4.23	6.77	0.16		1.39/4.55	5.94			
1000°C, 2 Kb, $fH2^b$ = 31 bar, water saturated, 16 days														
4/1	73.70	11.47	0.61	0.01	3.70	4.57	6.25	0.04		1.35/3.77	5.12	0.52	0.11	0.09
4/2	73.20	11.50	0.98	0.00	3.80	4.53	5.95	0.055		n.d.	n.d.	0.79	0.21	0.12
4/3	72.37	11.48	1.22	0.02	3.78	4.60	6.35	0.07		1.34/3.91	5.24	0.97	0.28	0.13
4/4	72.82	10.98	1.81	0.03	3.40	4.63	6.09	0.095		1.34/3.97	5.32	1.39	0.47	0.15
4/5	72.10	10.45	3.12	0.02	3.57	4.29	6.01	0.12		1.26/4.00	5.26	2.40	0.80	0.15
4/6	71.16	11.10	4.65	0.00	3.18	3.79	5.01	0.14		1.23/3.84	5.07	3.68	1.08	0.13
4/7	69.21	11.64	6.37	0.03	3.32	4.14	4.36	0.16		1.06/3.43	4.49	4.90	1.64	0.15
4/8	68.29	11.82	7.18	0.00	3.47	4.06	4.22	0.165		1.04/3.46	4.50	5.59	1.77	0.14
1000°C, 2 Kb, $fH2^b$ = 22 bar, water saturated, 10 days														
5/1	68.38	11.71	5.43	0.02	3.65	4.45	5.10	0.16		n.d.	n.d.	4.00	1.59	0.18
5/2	67.16	11.28	7.93	0.01	3.51	3.97	4.50	0.17		n.d.	n.d.	6.15	1.97	0.14
1000°C, 2 Kb, fH2 = 2.4 bar, water saturated, 6 days														
6/1	73.46	10.90	0.44	0.01	3.66	4.75	6.68	0.01		n.d.	n.d.	0.33	0.12	0.16
6/2	72.80	11.25	0.77	0.06	3.48	4.56	6.97	0.01		n.d.	n.d.	0.55	0.25	0.20
6/3	72.01	11.46	1.71	0.00	3.55	4.57	6.58	0.03		n.d.	n.d.	1.05	0.73	0.31
6/4	72.33	10.54	2.20	0.01	3.42	4.41	6.97	0.03		n.d.	n.d.	1.26	1.04	0.37
6/5	72.25	10.45	2.71	0.03	2.93	4.37	7.15	0.04		n.d.	n.d.	1.46	1.39	0.43
6/5-Mt		1.89	88.73											
6/6	70.96	11.83	2.86	0.02	3.03	4.39	6.80	0.03		n.d.	n.d.	1.86	1.11	0.27
6/6-Mt		3.02	87.70											
6/7	73.61	11.16	0.41	0.02	3.72	4.78	6.05			1.50/4.04	5.54	0.31	0.12	0.17
6/8	72.80	11.48	0.82	0.01	3.65	4.51	6.20			1.45/3.98	5.43	0.60	0.25	0.18
6/9	71.90	11.49	1.86	0.00	3.60	4.61	6.40			1.31/3.95	5.26	1.13	0.81	0.32
6/10	72.29	10.76	2.42	0.02	3.48	4.44	6.38			1.24/3.99	5.23	1.35	1.19	0.40
6/11	72.15	10.68	2.93	0.01	3.17	4.38	6.45			n.d.	n.d.	2.00/1.68	2.42/1.68	0.45
6/11-Mt		1.82	88.85											
6/12	71.18	11.43	2.97	0.02	3.18	4.25	6.81			n.d.	n.d.	3.09/1.93	4.35/1.16	0.27
6/12-Mt		2.94	87.93											
7														
7/1-gl	70.22	14.93	3.77	2.50	3.43	3.18	–					0.78	3.32	1.91
7/1-HM		6.24	82.09											
7/2-gl	73.26	13.08	3.23	1.78	2.96	3.59	–					0.68	2.83	1.87
7/2-HM		5.16	82.28											

Methods	EMPA									FTIR		Wet Chemistry		
Phases	Glasses or Oxides when specified							Alloys		Glasses				
# Sample	SiO_2	Al_2O_3	FeO	CaO	Na_2O	K_2O	H_2O	X $Fe^{(Ir)}$	X $Fe^{(Pt)}$	OH/H_2O	H_2O	FeO wt%	Fe_2O_3	X Fe_2O_3/XFeO
7/3-gl	75.29	11.86	2.73	0.85	3.14	4.15	-					0.54	2.43	2.02
7/3-HM		3.81	84.01											
7/4-gl	75.18	12.19	2.45	0.02	3.48	4.63	-					0.52	2.14	1.85
7/4-HM		3.95	83.94											
1300°C, 0.001 Kb, air, 25 days														
8/1-gl	75.14	11.56	3.85	0.84	3.03	4.08	-					0.77	3.42	2.00
8/1-HM		3.56	84.75											
8/2-gl	72.91	12.78	4.28	1.63	2.93	3.62	-					1.07	3.57	1.50
8/2-HM		4.78	82.77											
8/3-gl	75.03	11.93	3.15	0.01	3.40	4.65	-					0.73	2.69	1.66
8/3-HM		3.96	83.39											
1160°C, 2 Kb, $fH2^b$ = 0.1 bar, water saturated, 4 days														
9/1-gl	71.41	10.96	2.00	0.04	3.30	4.53	5.73			n.d.	n.d.	0.54	1.62	1.35
9/2-gl	70.83	10.89	2.99	0.05	3.26	4.48	6.06			n.d.	n.d.	0.70	2.55	1.64
9/2-HM		1.60	85.32											
9/3-gl	70.82	10.80	2.96	0.02	3.15	4.56	5.79			n.d.	n.d.	0.72	2.49	1.56
9/3-HM		1.69	86.45											
9/4-gl	70.83	10.80	2.99	0.00	3.19	4.50	5.77			n.d.	n.d.	0.73	2.51	1.55
9/4-HM		1.66	85.24											
9/5-gl	70.71	10.97	2.87	0.79	2.92	3.89	5.55			n.d.	n.d.	0.84	2.26	1.21
9/5-HM		1.93	86.38											
9/6-gl	69.75	11.81	2.68	1.66	2.80	3.44	5.58			n.d.	n.d.	0.85	2.03	1.08
9/6-HM		2.69	86.40											
9/7-gl	70.96	10.89	2.40	0.03	3.47	4.58	5.84			n.d.	n.d.	0.68	1.91	1.26
9/7-HM		1.60	85.32											

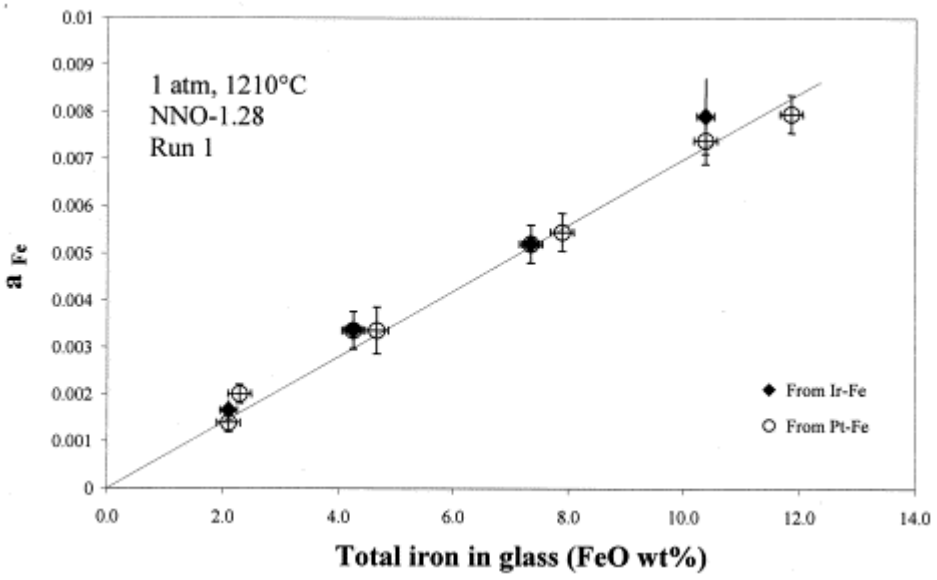

Fig. 5. Evidence for the consistency between Fe-metal activities calculated from Pt-Fe and, when available, Ir-Fe alloys. The total iron content of the melts is plotted against the calculated Fe metal activities that define, within error bars, a single trend. # Run 1, see Table 4 and Table 5 for data.

5.1.2. 2 kbar experiments

Results from the time-series experiments conducted with Ir wires are illustrated in Figure 6. At 1000°C, 2 kbar and for H_2O-saturated conditions, nearly flat Fe profiles in the Ir wire are obtained for durations of 25 d (Fig. 6c). For shorter durations, bulk equilibrium is clearly not attained. However, there is no gradient in Fe concentration in the melt adjacent to the Ir wire. The Fe contents at the metal-melt interface are reproducible, suggesting local equilibrium between metal and melt (run # 4 and 5, Table 4, see also Fig. 6a, 6b). In comparison,

experiments performed with Ir powders attained equilibrium much more rapidly. Under the same conditions as above (1000°C, 2 kbar, H_2O saturation), homogeneous Fe concentrations in Ir-Fe alloys were obtained after 6 d (run # 3, Table 4, Fig. 7). The establishment of ferric-ferrous equilibria in hydrous silicic melts requires only a few hours at 800–1000°C [Gaillard et al., 2002]. In contrast, Fe loss to the capsule may require a significant amount of time because of a high container/sample mass ratio that makes the Fe mass transfer important. At fO_2 << NNO (run # 3, Table 4), Fe losses of about 50% were encountered for charges with the highest capsule/melt weight ratios. However, the Fe profile (Fig. 8) indicates that the Au capsule is homogeneous and there is no gradient in glass Fe concentrations at the interface (Fig. 8), suggesting equilibrium between Au capsule and glass. Therefore, alloying of Fe in the noble metal capsules does not delay significantly the attainment of equilibrium between Ir-Fe alloys and melt.

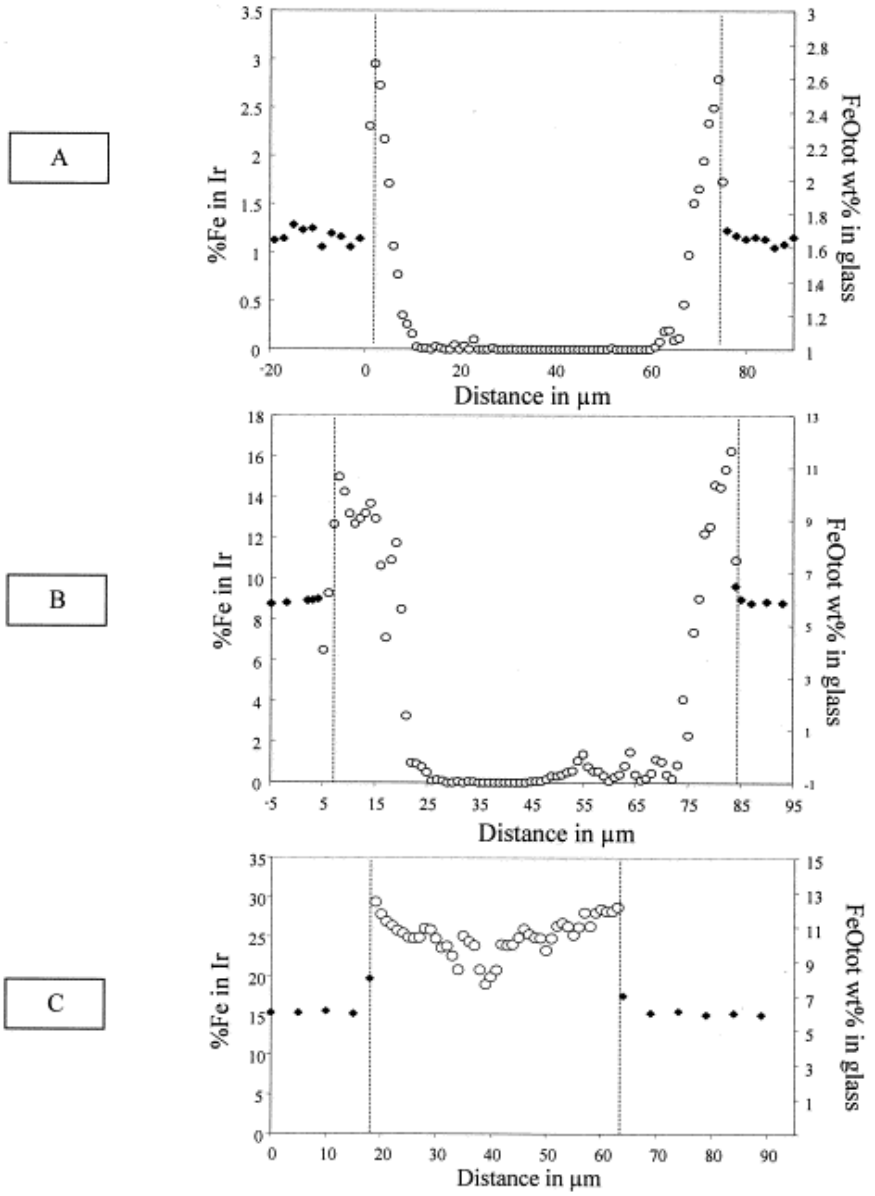

Fig. 6. Melt Fe-Ir interactions at 2 kb, 1000°C and water saturation illustrated by chemical profiles at the melt-Ir boundary. Non equilibrated after 4 days (A, run non-tabulated) and 10 days (B, sample #5/9 see Table 4 and Table 5):; (C): Nearly equilibrated after 25 days (run non-tabulated because the redox sensor was polluted by sulfide and subsequently unusable).

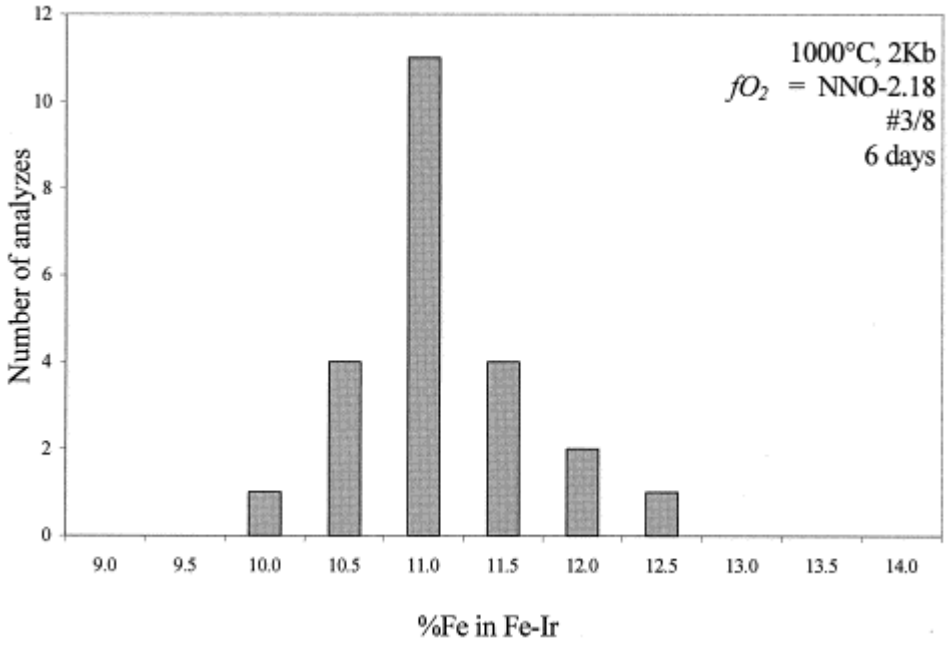

Fig. 7. Histogram of Fe content in 23 analysed Fe-Ir grains of the charge #3/8. The experiment lasts 6 days (See Table 4 and Table 5).

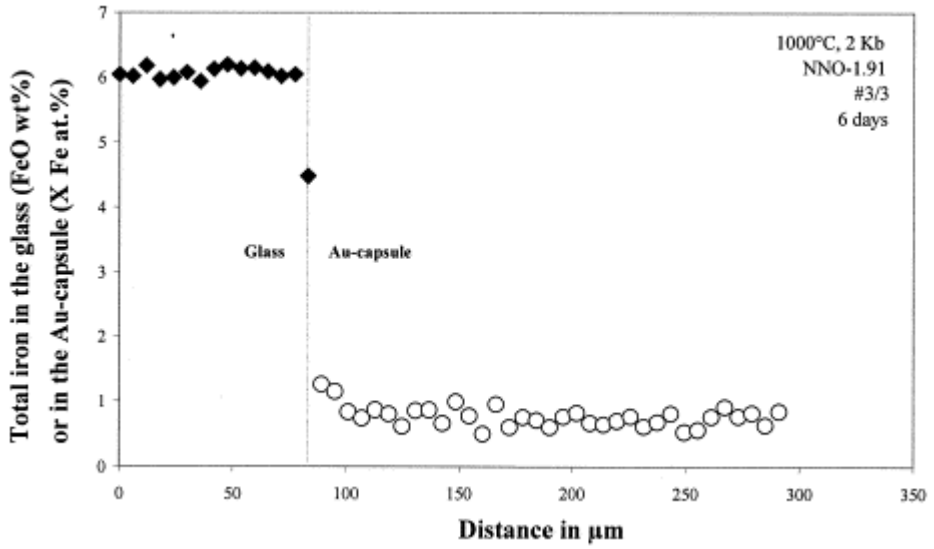

Fig. 8. Evidence of equilibrium attainment between melt and Au-capsule after 6 days-long experiments. Sample #3/3 (see Table 4 and Table 5).

Activities of FeO^{liq} and $Fe_2O_3{}^{liq}$ were also calculated from independent equilibria. In sample # 2/7 (run # 2, Table 4), results obtained from both activity sensors (Pt capsule and Ir powders) are nearly identical (difference of $\sim$1400 Joules, Table 4) and suggest attainment of equilibrium between metal and melt because the Pt capsule and Ir powders are physically separated by the melt. Another test is provided by the magnetite-bearing charges of run # 6 (Table 4). Activities of FeO^{liq} and $Fe_2O_3{}^{liq}$ were calculated from both the metal-melt (Eqn. 1) and magnetite-melt equilibria (i.e., Fe_3O_4 243 $\Leftrightarrow$3 FeO + $\frac{1}{2}O_2$). For the latter, standard state properties were taken from Table 1 and [Lange and Carmichael, 1990] for FeO^{liq}, whereas for Fe_3O_4, standard state and mixing properties where calculated from [Ghiorso and Sack, 1991]

and their composition was determined by EMPA. Results show that a_{FeO}^{liq} and a_{Fe2O3}^{liq} are within 10% from each other (samples #6/5, #6/6, Table 4), which is evidence for equilibration of the different iron components between magnetite, Ir-Fe alloy, and melt. The activity of the magnetite component in these crystals, calculated with [Ghiorso and Sack, 1991], are nearly identical to those calculated from magnetite-metal equilibrium (i.e., Fe_3O_4 243 ⇔3 Fe + 2 O_2). This conclusion demonstrates the internal consistency of the thermodynamic database used to evaluate μ_{FeO}^{liq}, μ_{Fe2O3}^{liq}, μ_{Fe}^{alloy} and $\mu_{Fe3O4}^{magnetite}$.

5.1.3. Global vs. partial equilibrium

In the above section, we have presented evidence for the attainment of metal-melt, hematite-melt, magnetite-melt and magnetite-metal equilibria. It is worth stressing that this applies only to the different iron components (metallic iron in alloy, iron oxide components in melt, magnetite component in magnetite). Global equilibrium (defined as the equality of the chemical potential (μ_i^{Φ}) of each component (i) in each phase (Φ)) is not claimed. The absence of Ir in suspension wires or containers and, conversely, the absence of Au, Pt, or Pd in the Ir-Fe alloys is evidence for some disequilibrium in our experiments. Noble metals have very low solubilities in silicate melts (e.g., [O'Neill et al., 1995], which would limit the flux of noble metals and make their equilibration through the melt over long distances difficult. Although it is quite likely that equilibrium for the noble metals is attained locally between melt and either alloys or suspension wires or containers, equilibrium is clearly not attained between the various noble metal phases, and therefore global equilibrium is not attained. However, partial equilibrium is demonstrated for the different iron components and this is all what is needed for the measurement of their activities.

To illustrate this point, ternary Pt-Ir-Fe alloys were obtained in an experiment performed at high temperatures (1380°C), 1 atm and for 10 d at FMQ. The charge, made of a basaltic composition containing 8.04 wt.% FeO_{tot} plus Ir powders, was suspended to a Pt wire. A glass homogeneous in major elements was obtained (Table 3). Compositions of alloys were found to vary with their spatial position in the charge. Only Fe-Ir alloys were found in the main part of the glass. In a narrow zone (50 μm) near the Pt wire, alloys with ternary compositions were found. The composition in this zone varies from Ir-free (rim of the Pt wire) to Pt-free (the farther away from the Pt wire, Fig. 9). The experiment is thus out of global equilibrium. Yet, a_{FeO}^{liq} calculated from each end-member binary composition (i.e., Ir-free and Pt-free) are nearly identical (respectively 0.077 and 0.081), suggesting that partial metal-melt equilibrium is attained for the Fe^{metal} and FeO^{liq} components. Differences in alloy Fe contents (Fig. 9) are not ascribed to variations of μ_{FeO}^{liq} but rather result from changes in the mixing properties of the alloy controlled by the local Pt/Ir ratio. These ternary alloys were not found in other run products. This is probably due to difference in both run duration and temperature and in viscosity of melts that would affect the flux of noble metals and, therefore, the communication of their chemical potential. Nevertheless, we show that the absence of global equilibrium does not invalidate measurements of molten iron oxides activities.

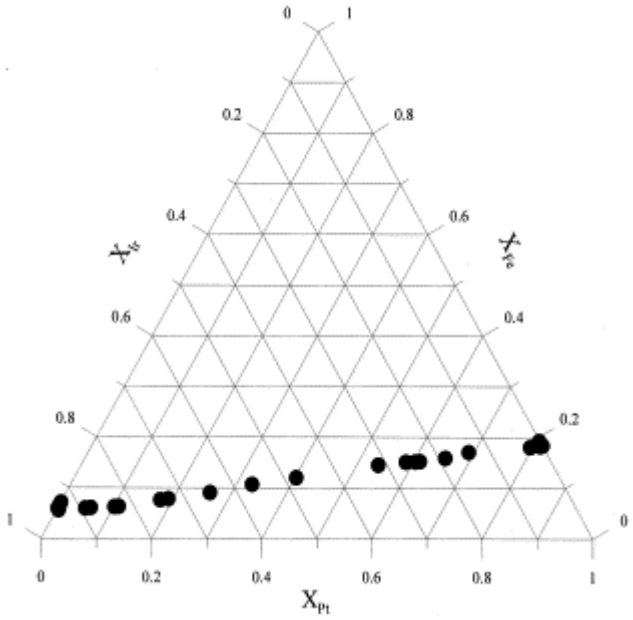

Fig. 9. Non-equilibrated Fe-Ir-Pt alloys and the effect of Pt/Ir on the Fe content of the alloys. The values of a_{FeO}^{liq} were calculated from the fO_2 and the composition of Ir-Fe binary (left, $a_{FeO}^{liq} = 0.081$) and Pt-Fe binary (right, $a_{FeO}^{liq} = 0.077$). See Table 3 and text (5.1.3).

5.2. Activity results

The experimental conditions are presented together with the activities of FeO^{liq} and $Fe_2O_3^{liq}$ (a_{FeO}^{liq}, a_{Fe2O3}^{liq}) in Table 4. The tabulated experiments satisfy to the conditions of equilibrium, except for runs # 4 and 5 (local metal-melt equilibrium, see above and Fig. 6). Neither non-equilibrated time-series experiments nor runs having experienced failure of the Co-Ni-Pd redox sensor are reported. The electron microprobe data for glasses, hematite, magnetite and alloys, together with the determinations of H_2O contents and the Fe^{3+}/Fe^{2+} data are given in Table 5. For the calculation of the mole fractions of FeO^{liq} and $Fe_2O_3^{liq}$ (X_{FeO}^{liq} and X_{Fe2O3}^{liq}), the melt compositions were recast in terms of the following components: Si_4O_8, $KAlO_2$, $NaAlO_2$, $CaAl_2O_4$, Al_2O_3, CaO, H_2O, OH, FeO, Fe_2O_3. Glasses in experiments performed with the Ca-free starting compositions have various FeO_{tot} but nearly identical Si_4O_8, $KAlO_2$ and $NaAlO_2$ contents and all but 1 or 2 are peraluminous (Table 5). Therefore, a_{FeO}^{liq} and a_{Fe2O3}^{liq} are varied at constant composition of the aluminosilicate matrix. In experiments performed with the Ca-bearing starting compositions, variations in a_{FeO}^{liq} and a_{Fe2O3}^{liq} are coupled with differences in the composition of the aluminosilicate matrix.

5.2.1. The effect of water on a_{FeO}^{liq} and a_{Fe2O3}^{liq}

For moderately reducing conditions (i.e., from NNO - 1 to NNO - 1.5) and under anhydrous conditions at 1210°C (run # 1), glass FeO_{tot} ranges between 2.10 and 11.85 wt.% (Table 5). Iron redox ratios ($XFe_2O_3/XFeO$) are very low (from 0.01 to 0.07) and positively correlated with FeO_{tot} (Table 5). The activity-composition relations for the anhydrous melts are shown in Figure 10. The agreement between activities determined from either the Ir-Fe or Pt-Fe (suspension wire) sensors is excellent. The anhydrous data show that a_{FeO}^{liq} we measured is very close to the activities determined by [Doyle, 1988] (straight line in Fig. 10) with $\gamma_{FeO}^{liq} = 0.7$ ($\gamma_{FeO}^{liq} = a_{FeO}^{liq}/X_{FeO}^{liq}$. The very good agreement between the Doyle's and our a_{FeO}^{liq} emphasizes the consistency between our research and the previous studies devoted to

measurement of thermodynamic properties of molten iron oxides in silicate melts. The effect of the addition of H_2O is apparent from run # 2 performed at 1160°C, 2 kbar, and under fO_2 conditions, NNO−1.25, very close to that of run # 1 (Table 4). The glasses (1.78 - 10.64 wt.% FeO_{tot}) have H_2O concentrations ranging from 4.96 to 5.61 wt.% (Table 5). The redox ratios of iron in these glasses (0.05 to 0.13) are significantly higher than in run # 1, although the fO_2 is nearly similar, and show a positive correlation with FeO_{tot} (see also [Gaillard et al., 2001]. Activities of FeO^{liq} follow Henry's law but a_{FeO}^{liq} is higher in the hydrous than in the anhydrous samples at a given X_{FeO}^{liq} (with $\gamma_{FeO}^{liq} = 0.7$ for anhydrous samples against 1 for the hydrous series). In contrast, for $Fe_2O_3^{liq}$ (Fig. 11), addition of H_2O decreases a_{Fe2O3}^{liq} at a given X_{Fe2O3}^{liq} in comparison with a_{Fe2O3}^{liq} of anhydrous glasses under similar T-fO_2 conditions. The combined effect of water on a_{FeO}^{liq} and a_{Fe2O3}^{liq} implies that the ratio $\gamma_{Fe2O3}^{liq}/\gamma_{FeO}^{liq}$ is lower in hydrous than in anhydrous melts. This observation is consistent with the increase of the iron redox ratio ($XFe_2O_3/XFeO$) noted above for the hydrous glasses from run # 2 in comparison with the anhydrous glasses from run # 1 (see also [Baker and Rutherford, 1996 and Gaillard et al., 2001].

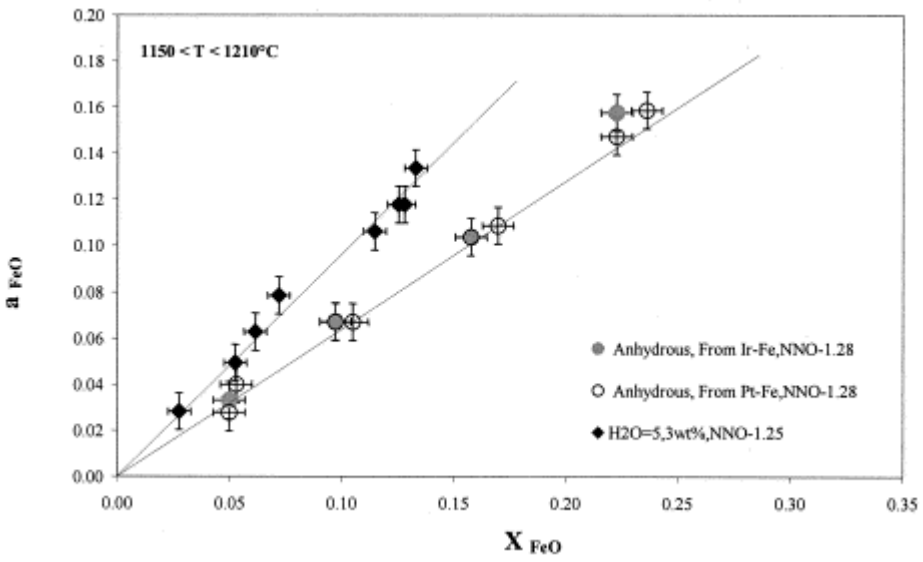

Fig. 10. Activity-compositions relationship for FeO^{liq} in anhydrous and hydrous melts under reducing conditions (Data extracted from # Runs 1-2, see Table 4 and Table 5). For the anhydrous compositions, a_{FeO}^{liq} are calculated from both Ir-Fe and Pt-Fe liquid equilibria. The straight line passing through the one atm data is an extrapolation of a_{FeO}^{liq} measured by Doyle et al. (1989).

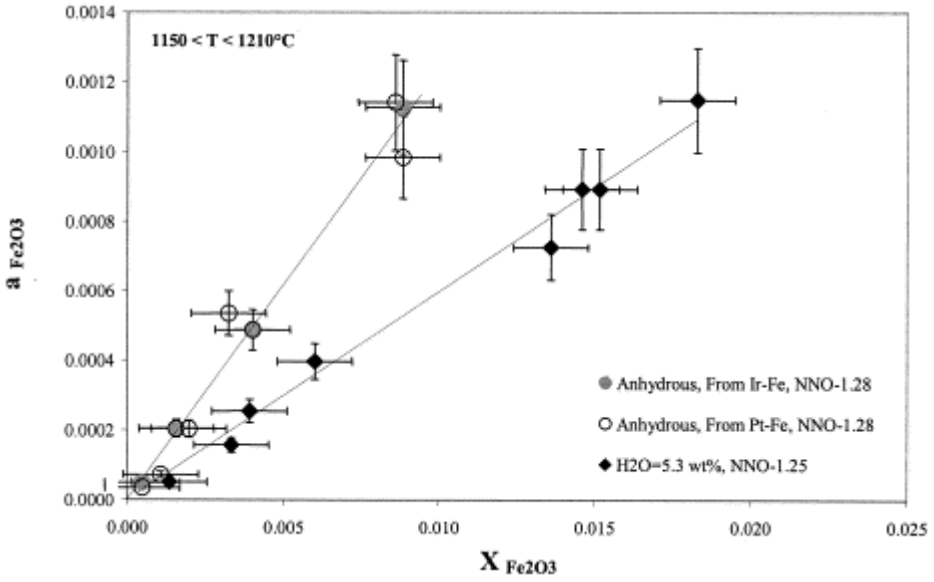

Fig. 11. Activity-compositions relationship for $Fe_2O_3^{liq}$ in anhydrous and hydrous melts under reducing conditions (Data extracted from # Runs 1-2, see Table 4 and Table 5). For the anhydrous compositions, a_{FeO}^{liq} are calculated from both Ir-Fe and Pt-Fe liquid equilibria.

Constraints on the effect of H_2O on a_{FeO}^{liq} under isobaric conditions (2 kbar) are provided by run # 3 (Table 4). Glass H_2O contents range between 2.40 to 6.65 wt.% (Table 4–5). Because of variations in H_2O concentration (and hence in fH_2O), fO_2 differs between samples, from NNO−1.91 to NNO−3.16 (Table 4). Under these conditions, very little Fe is present as Fe^{3+} and glass FeO_{tot} (0.70–7.46 wt.%) are equivalent to their FeO concentrations. For all samples from runs # 1–3, the excess chemical potential of FeO^{liq} ($\mu^{xs}_{FeO}{}^{liq} = RT \ln \gamma_{FeO}^{liq}$) is plotted against the water content (Fig. 12). Despite differences in T, P, fO_2 and FeO_{tot} between samples, the data consistently show that the addition of water progressively increases $\mu^{xs}_{FeO}{}^{liq}$. The deviation from ideality changes from negative at low and intermediate water contents to slightly positive above ~5 wt.% H_2O (Fig. 12).

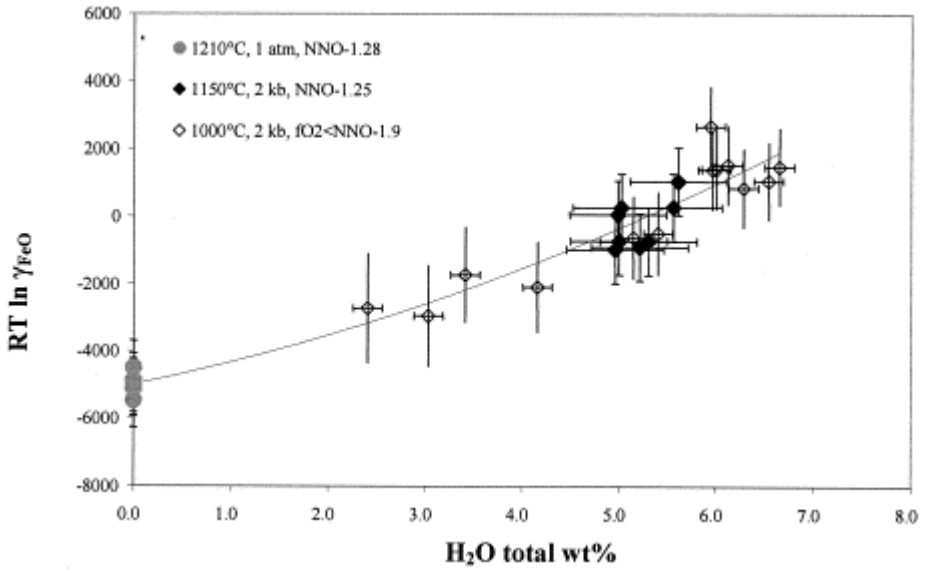

Fig. 12. Excess chemical potential of FeO^{liq} as a function of the water content under reducing conditions (Data extracted from # Runs 1-2-3, see Table 4 and Table 5). Water content is determined by difference on EMPA (black diamond-shaped) and FTIR (hollow diamond-shaped). The curve is a polynomial fit on the data.

Under strongly oxidizing conditions (NNO+4.9 < fO_2 < NNO+7.3), the glasses are characterized by a narrow range of FeO_{tot} (2.45–3.15 wt.%) reflecting saturation with hematite (samples # 7/4, 8/3, 9/2 to 9/4, note that sample 9/1 is undersaturated in hematite, Table 4). In detail, the hydrous glasses saturated with respect to hematite at 1160°C have a higher FeO_{tot} than the anhydrous glasses at 1245°C, which shows that water (in the range 5.55 to 6.06 wt.% H_2O, Table 5) increases the solubility of hematite at high fO_2. For both series, glasses are strongly oxidized ($XFe_2O_3/XFeO$ = 1.55–1.85, Table 5) and it is difficult to identify any effect of water on the ferric-ferrous ratio. The excess chemical potential of FeO^{liq} indicates positive deviation from ideality and seems slightly higher in the hydrous than in the anhydrous melts (Fig. 13). However, because glass FeO contents are low under such oxidizing conditions, errors in the determination of X_{FeO}^{liq} are important making estimation of the effect of water difficult. Excess chemical potentials of $Fe_2O_3^{liq}$ for hydrous and anhydrous melt overlap, so that the effect of water on γ_{Fe2O3}^{liq} for strongly oxidizing fO_2 is not very marked (Fig. 14).

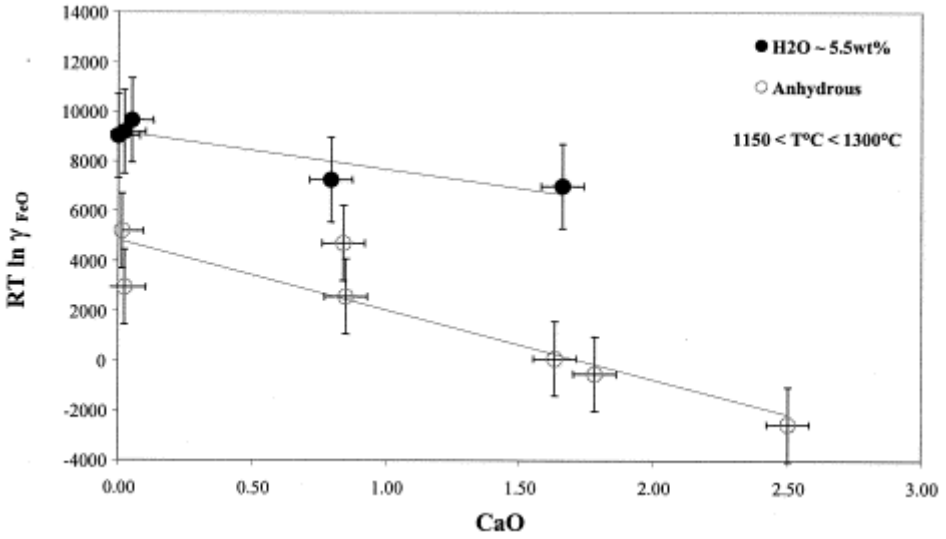

Fig. 13. Excess chemical potential of FeO^{liq} as a function of the calcium content under oxidizing conditions (Data extracted from # Runs 7-8-9, see Table 4 and Table 5).

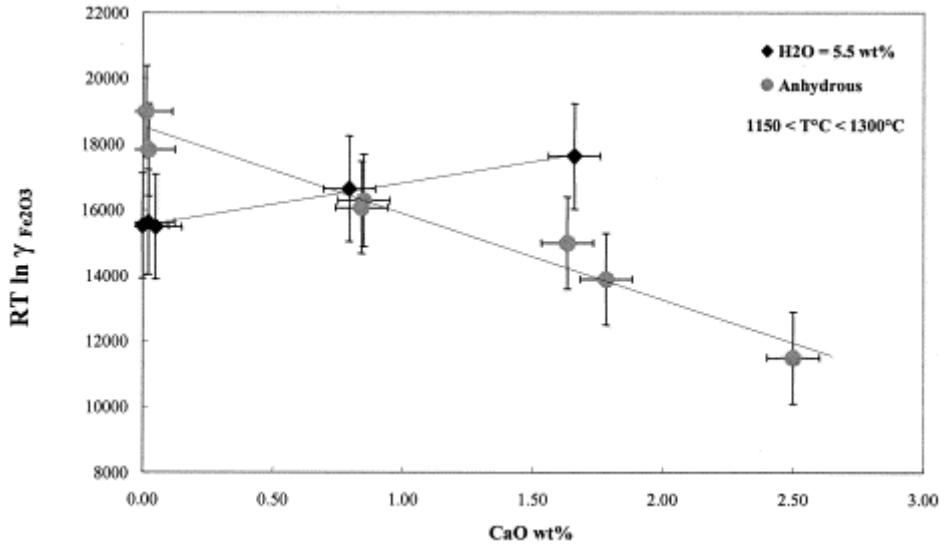

Fig. 14. Excess chemical potential of $Fe_2O_3^{liq}$ as a function of the calcium content under oxidizing conditions (Data extracted from # Runs 7-8-9, see Table 4 and Table 5).

The FTIR results reveal that the water solubility decreases with increasing iron content. This is particularly obvious for runs 4 and 6 (Table 5) where the water solubility decreases from 5.2 to 4.5 wt.% as iron content varies from 0.6 to 7.2 wt.% FeO. However, because the effect of iron content on the extinction coefficient of OH and H_2O bands in glass is currently unknown, we consider that this observation, to be interpreted, needs confirmation by an independent method of water content measurement, which is beyond the scope of this study.

5.2.2. The effect of fO_2 on a_{FeO}^{liq} and a_{Fe2O3}^{liq} of hydrous melts

Redox conditions dominate the activities of both FeO^{liq} and $Fe_2O_3^{liq}$ in H_2O-saturated melts synthesized at 2 kbar. For FeO^{liq}, activity-composition relationships are shown in Figure 15 for 4 fO_2 ranging from NNO−1.25 to NNO+4.9, and at 2 temperatures (1000 and 1160°C). For all oxyisobars (O_2 isobars), a_{FeO}^{liq} follows Henry's behavior. The Henry's law constant (constant activity coefficient, γ_{FeO}^{liq}) is positively correlated with fO_2, increasing from a value of $\sim$1 at NNO−1.25 (see also Fig. 10) to $\sim$4 at NNO+1.4. The point for NNO+4.9 (which corresponds to 3 nearly identical measurements, run # 9, Table 4) clearly shows that the positive dependence of γ_{FeO}^{liq} on fO_2 does not apply for fO_2 above NNO+1.4. There should exist a maximum in γ_{FeO}^{liq} for a fO_2 between NNO+1.4 and NNO+4.9. Activity-composition relationships for $Fe_2O_3^{liq}$ are shown on Figure 16. As observed for FeO^{liq}, γ_{Fe2O3}^{liq} has positive fO_2 dependence. The a_{Fe2O3}^{liq} - X_{Fe2O3}^{liq} relationships, which are nearly ideal at NNO+1.4, show a strong negative deviation at NNO−1.25. At NNO−0.8 and NNO+1.4, a_{Fe2O3}^{liq} does not vary linearly with X_{Fe2O3}^{liq} and therefore $Fe_2O_3^{liq}$ does not follow Henry's law in the entire fO_2 range covered by Figure 16. The point at NNO+4.9 (run # 9, Table 4) plots well outside Figure 16 (a_{Fe2O3}^{liq} = 0.069–0.070 for X_{Fe2O3}^{liq} = 0.02). This demonstrates that the increase of γ_{Fe2O3}^{liq} with fO_2 continues above NNO+1.4, in contrast to the behavior of FeO^{liq}.

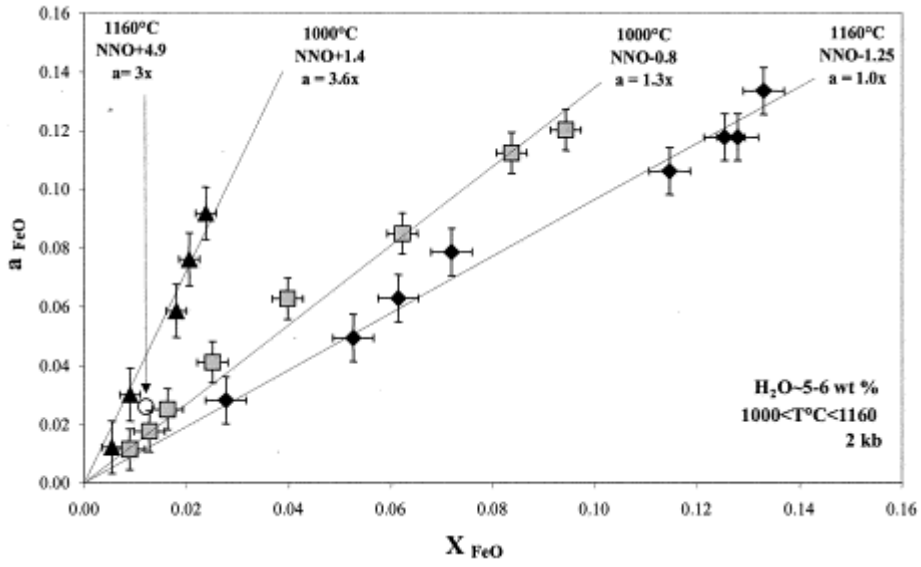

Fig. 15. The effect of fO_2 on activity-composition relationships for *FeO^{liq}* in H_2O-saturated melts at 2 kb. Data are extracted from # Runs 2-4-6-9 (See Table 4 and Table 5). The lines are best fit to the iso-fO_2 data and the resulting a-X relationships are given.

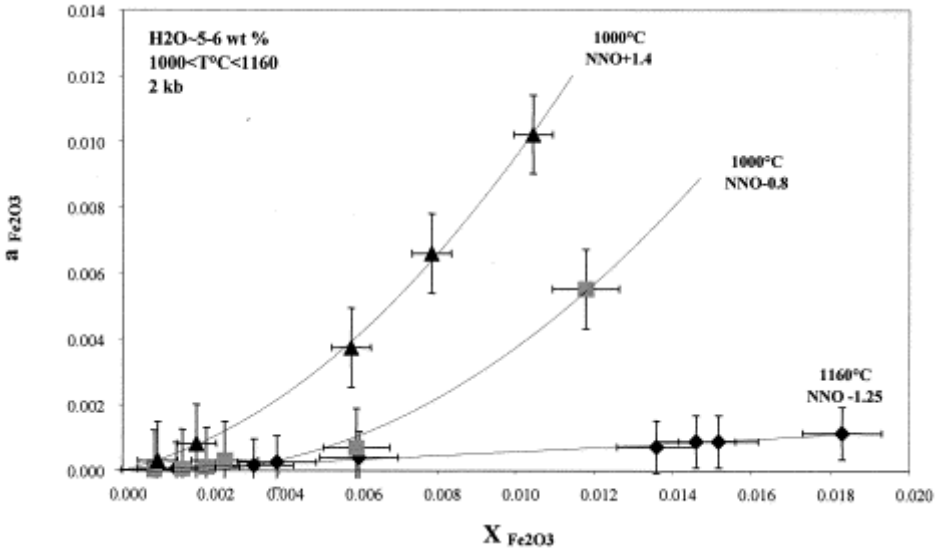

Fig. 16. The effect of fO_2 on activity-composition relationships for $Fe_2O_3^{liq}$ in H_2O-saturated melts at 2 kb. Data are extracted from # Runs 2-4-6 (See Table 4 and Table 5). Results from # Run 9 are not plotted here since it would have drastically changed the scale (see text).

5.2.3. The effect of Ca on a_{FeO}^{liq} and a_{Fe2O3}^{liq}

Comparison between the Ca-free and Ca-bearing runs at high fO2 (between NNO+4.9 and NNO+7.3) allows the effect of the Ca = K + Na substitution to be demonstrated (Fig. 13). Important differences appear between the 2 kbar hydrous and 1 atm anhydrous samples. FeOtot concentrations in hydrous glasses at equilibrium with hematite decrease with increasing CaO (run # 9, Table 4) whereas the reverse is observed for anhydrous glasses (runs # 7, 8, Table 4). The ferric-ferrous ratio decreases with increasing CaO for the hydrous glasses (samples 9/2 to 9/6, Table 4) but does not vary significantly for anhydrous glasses (samples 7/1 to 7/4 and 8/1 to 8/3, Table 4). Excess chemical potentials of FeO^{liq} decrease with CaO for both hydrous and anhydrous compositions (Fig. 13), and the effect of water on $\mu^{xs}_{FeO}{}^{liq}$ appears to be more marked as CaO increases. In contrast, the effects of CaO on RT ln $\gamma_{Fe2O3}{}^{liq}$ for hydrous and anhydrous melts are barely distinguishable from each other except at the highest CaO concentrations (Fig. 14).

6. Discussion and conclusions

6.1. Water and $fe^{3+}/^{F}e^{2+}$

Here above we have put in evidence different effects of water on $a_{FeO}{}^{liq}$ and $a_{Fe2O3}{}^{liq}$ that are both fO_2 dependent. In terms of Fe_2O_3/FeO - fO_2 relationships, our results suggest that water addition increases ferric/ferrous under reducing conditions and has a less important or no effect under oxidizing conditions. This is in very good agreement with previous experimental studies [Baker and Rutherford, 1996 and Gaillard et al., 2001] identifying similar effects of water. The recent results of [Wilke et al., 2002] do not follow this trend probably due to the Na-poor and Ca-rich composition they used. Our results indeed suggest that substitution of Na by Ca should increase the activity coefficient of ferric iron in hydrous melts and therefore decreases the Fe^{3+}/Fe^{2+} of the melt. Such an effect of Ca on Fe^{3+}/Fe^{2+} of hydrous melt was also identified by [Gaillard et al., 2001] on the Pinatubo glass matrix sample. The results of

[Moore et al., 1995] do not follow the trend we observed. Indeed, their conclusions suggested that water has no measurable effect on Fe^{3+}/Fe^{2+} of silicate melts. However, their experiments were essentially conducted on peralkaline melts in contrast to our and [Baker and Rutherford, 1996]'s studies that concern metaluminous systems. We therefore anticipate that the conclusions we draw about the effect of water on the energetic of molten iron oxides in metaluminous melts cannot be extrapolated to peralkaline molten silicates.

6.2. Conclusive remarks

The effect of water and fO_2 on a-X relationships in rhyolitic melts has been elucidated by equilibrating Fe-Ir, Fe-Pt alloys and hematite with molten silicates. We showed that under reducing conditions, water increases the activity coefficient of ferrous iron and has an opposite effect on ferric iron. Therefore, water incorporation in melts under reducing conditions result in a slight increase of Fe^{3+}/Fe^{2+}. Under oxidizing conditions, no significant effect of water can be measured. In contrast, a-X relationships for both ferrous and ferric iron components are strongly positively deviated as fO_2 increases. For FeO^{liq}, activity coefficient changes from ideality at QFM to $\sim$4 at NNO+1.5. Combining these results with the previous works, a database covering compositions and conditions encountered in natural magmas is available. ([Alberto et al., 1992]; [Johnson et al., 1994])

Acknowledgements

This study, which is part of Fabrice Gaillard's PhD thesis, was supported by the Région Centre and by the EC TMR network "Hydrous Silicate Melts". The constructive reviews of Rebecca Lange and an anonymous scientist are acknowledged. Bjorn Mysen, who did the editorial work and his own review, is also greatly thanked.

References

Alberto et al., 1992. H.V. Alberto, J.M. Gil, N. Ayres DeCampos and B.O. Mysen, Redox equilibria of iron in Ti-bearing calcium silicate quenched glasses. *J. Noncryst. Sol.* **151** (1992), pp. 39–50.

Amossé and Alibert, 1993. J. Amossé and M. Alibert, Partitioning of iridium and platinum between metals and silicate melts: Evidence for passivation of the metals depending on fO_2. *Geochim. Cosmochim. Acta* **57** (1993), pp. 2395–2398.

Ariskin, 1999. A.A. Ariskin, Phase equilibria modeling in igneous petrology: Use of COMAGMAT model for simulating fractionation of ferro-basaltic magmas and the genesis of high-alumina basalt. *J. Volcanol. Geotherm. Res.* **90** (1999), pp. 115–162.

Baker and Rutherford, 1996. L. Baker and M.J. Rutherford, The effect of dissolved water on the oxidation state of silicic melts. *Geochim. Cosmochim. Acta* **60** (1996), pp. 2179–2187.

Banya et al 1980. Banya S., Chiba A., and Hikosaka A. (1980) Thermodynamic table for inorganic substances. Testu to Hagane, 1484

Barin 1998. Barin I. (1998) Thermochemical data of pure substances. VCH, Weinheim, Basel, Cambridge

Behrens and Jantos, 2001. H. Behrens and N. Jantos, The effect of anhydrous composition on water solubility in granitic melts. *Am. Mineral.* **86** (2001), pp. 14–20.

Berman and Brown, 1984. R.G. Berman and T.H. Brown, A thermodynamic model for multicomponent melts with application to the system CaO-Al_2O_3-SiO_2. *Geochim. Cosmochim. Acta* **48** (1984), pp. 661–678.

Berman and Brown, 1987. Berman R. G. and Brown T. H. (1987) Development of model for multicomponent melts: Analysis of synthetic systems. *Revs. Mineralogy* **17,** 405–442

Bodsworth, 1959. C. Bodsworth, The activity of ferrous oxide in silicate melts. *Iron Steel Inst. J.* **193** (1959), pp. 13–24.

Bowen and Schairer, 1934. N.L. Bowen and J.F. Schairer, The system MgO-FeO-SiO_2. *Am. J. Sci.* **29** (1934), pp. 151–217.

Burnham et al., 1969. C.W. Burnham, J.R. Holloway and N.F. Davis, Thermodynamic property of water to 1000°C and 10000 bar. *Geological Society of America Special Paper* **132** (1969), pp. 1–96.

Carmichael, 1991. I.S.E. Carmichael, The redox state states of basic and silicic magmas: A reflection of their source regions. *Contrib. Mineral. Petrol.* **106** (1991), pp. 129–141.

Coughlin, 1954. Coughlin J. P (1954) Contribution to the data of theoretical metallurgy, XII, heats and free energies of formation of inorganic oxides. U. S. Bur. Mines. Bull. 542

DeCapitani and Kirschen, 1998. C. DeCapitani and M. Kirschen, A generalized multicomponent excess function with application to immiscible liquids in the system CaO-SiO_2-TiO_2. *Geochim. Cosmochim. Acta* **62** (1998), pp. 3753–3763.

Deines et al., 1974. Deines P., Nafziger R. H., Ulmer G. C., and Woermann E. (1974) Temperature oxygen fugacity tables for selected gas mixture in the system C-O-H at one atmosphere total pressure. Bulletin of the Earth and Mineral Sciences Station 88, The Pennsylvania State University

Devine et al., 1995. J.D. Devine, J.E. Gardner, H.P. Brach, G.D. Layne and M.J. Rutherford, Comparison of microanalytical methods for estimation of H_2O content of silicic volcanic glasses. *Am. Mineral.* **80** (1995), pp. 319–328.

Doyle, 1988. C.D. Doyle, Prediction of the activity of FeO in multicomponent magma from known values in [SiO_2-$KAlO_2$-$CaAl_2Si_2O_8$]- FeO liquids . *Geochim. Cosmochim. Acta* **52** (1988), pp. 1827–1834.

Doyle, 1989. C.D. Doyle, The effect of substitution of TiO_2 for SiO_2 on a FeO in magma. *Geochim. Cosmochim. Acta* **53** (1989), pp. 2631–2638.

Doyle and Naldrett, 1986. C.D. Doyle and A.J. Naldrett, Ideal mixing of divalent cations in mafic magma and its effect on the solution of ferrous oxide. *Geochim. Cosmochim. Acta* **50** (1986), pp. 435–443.

Eriksson and Pelton, 1993. G. Eriksson and A.D. Pelton, Critical evaluation and optimization of the thermodynamic properties and phase diagrams of the MnO-TiO_2, MgO-TiO_2, FeO-TiO_2, Ti2O3-TiO_2, Na_2O-TiO_2, and K_2O-TiO_2 systems. *Metal. Trans.* **24b** (1993), pp. 795–805.

Gaillard et al., 2001. F. Gaillard, B. Scaillet and M. Pichavant, The effect of water and fO_2 on the ferric-ferrous ratio of hydrous silicic melts. *Chem. Geol.* **174** (2001), pp. 255–273.

Gaillard et al., 2002. F. Gaillard, B. Scaillet and M. Pichavant, Kinetics of iron oxidation-reduction in hydrous silicic melts. *Am. Mineral.* **87** (2002), pp. 829–837.

Ghiorso and Sack, 1991. M.S. Ghiorso and R.O. Sack, Fe-Ti oxide geothermometry: Thermodynamic formulation and the estimation of intensive variables in silicic magmas. *Contrib. Mineral. Petrol.* **108** (1991), pp. 485–510.

Ghiorso and Sack, 1995. M.S. Ghiorso and R.O. Sack, Chemical mass transfer in magmatic processes: IV. A revised and internally consistent thermodynamic model for the interpolation and extrapolation of liquid-solid equilibria in magmatic systems at elevated temperatures and pressures. *Contrib. Mineral. Petrol.* **90** (1995), pp. 197–212.

Hamilton et al., 1964. D.L. Hamilton, C.W. Burnham and E.F. Osborn, The solubility of water and effects of oxygen fugacity and water content on crystallization in mafic magmas. *J. Petrol.* **5** (1964), pp. 21–39.

Heald, 1967. E.F. Heald, Thermodynamic of iron-platinum alloys. *Trans. Metallurgical Soc. AIME* **239** (1967), pp. 1337–1340.

Holzheid et al., 1997. A. Holzheid, H. Palme and S. Chakraborty, The activities of NiO and FeO in silicate melts. *Chem. Geol.* **139** (1997), pp. 21–38.

Johnson et al., 1994. Johnson M. C., Anderson A. T., and Rutherford M. J. (1994) Pre-eruptive volatile contents of magmas. *Revs. Mineralogy* **30,** 281–323

Kawamoto and Hirose, 1994. T. Kawamoto and K. Hirose, Au-Pd sample containers for melting experiments on iron and water bearing systems. *Eur. J. Min.* **6** (1994), pp. 381–385.

Kirschen and Pichavant, 2001. M. Kirschen and M. Pichavant, A thermodynamic model for hydrous silicate melts in the system $NaAlSi_3O_8$-$KAlSi_3O_8$-Si_4O_8-H_2O. *Chem. Geol.* **174** (2001), pp. 103–114.

Kress and Carmichael, 1991. V.C. Kress and I.S.E. Carmichael, The compressibility of silicate liquids containing Fe_2O_3 and the effect of composition: temperature, Oxygen fugacity and pressure on their redox states. *Contrib. Mineral. Petrol.* **108** (1991), pp. 82–92.

Lange and Carmichael, 1990. Lange R. A. and Carmichael I. S. E. (1990) Thermodynamic properties of silicate liquids with emphasis on density, thermal expansion and compressibility. *Revs. Mineralogy* **24,** 25–64

Lange and Navrotsky, 1992. R.A. Lange and A. Navrotsky, Heat capacity of Fe_2O_3-bearing silicate liquids. *Contrib. Mineral. Petrol.* **110** (1992), pp. 311–320.

Lapin et al., 1985. I.V. Lapin, O.A. Lukanin and A.A. Kadik, Effect of redox conditions on near-surface icelandic basalt crystallization and differentiation. *Geokhimya* **6** (1985), pp. 747–760.

Martel et al., 1999. C. Martel, M. Pichavant, F. Holtz, B. Scaillet, J.-L. Bourdier and H. Traineau, Effects of fO_2 and H_2O on andesite phase relations between 2 and 4 kbar. *J. Geophys. Res.* **104** (1999), pp. 453–470.

Massalski, 1992. Massalski T. B. (1992) *Binary Alloy Phase Diagrams.* (ed. P. R. Subramanian). Hardcover. American Society for metals, Ohio

Matsuzaki et al., 1998. K. Matsuzaki, Y. Higano, K. Katsumata and K. Ito, Activity measurement of FeOt-SiO_2-TiO_2-(CaO, MgO, AlO1.5) melts in equilibrium with solid iron. *Iron and Steel Institute of Japan* **38** (1998), pp. 1147–1149.

Moore et al., 1995. G. Moore, K. Righter and I.S.E. Carmichael, The effect of dissolved water on the oxidation state of iron in natural silicate liquids. *Contrib. Mineral. Petrol.* **120** (1995), pp. 170–179.

Mysen and Virgo, 1989. B.O. Mysen and D. Virgo, Redox equilibria: Structure and properties of Fe-bearing aluminosilicate melts: Relationships among temperature, composition, and oxygen fugacity in the system Na_2O-Al_2O_3-SiO_2-Fe-O. *Am. Mineral.* **74** (1989), pp. 58–76.

O'Neill, 1987a. H.S.t. C. O'Neill, Quartz fayalite iron and quartz fayalite magnetite equilibria and the free energy of formation of fayalite (Fe2SiO4) and magnetite (Fe_3O_4). *Am. Mineral.* **72** (1987), pp. 67–75.

O'Neill and Eggins, 2002. H.S.t. C. O'Neill and S.M. Eggins, The effect of melt composition on trace element partitioning: An experimental investigation of the activity coefficients of FeO, NiO, CoO, MoO2 and MoO3 in silicate melts. *Chem. Geol.* **186** (2002), pp. 151–181.

O'Neill et al., 1995. H.S.t. C. O'Neill, D.B. Dingwell, A. Borisov, B. Spettel and H. Palme, Experimental petrochemistry of some highly siderophile elements at high temperatures, and some implications for core formation and the mantle's early history. *Chem. Geol.* **120** (1995), pp. 255–273.

Osborn, 1959. E.F. Osborn, Role of oxygen pressure in the crystallization and differentiation of basaltic magma. *Am. J. Sci.* **257** (1959), pp. 609–647.

Pichavant, 1987. M. Pichavant, Effect of B and H_2O on liquidus phase relations in the haplogranite system at 1Kbar. *Am. Mineral.* **72** (1987), pp. 1056–1070.

Pichavant et al., 2002. M. Pichavant, C. Martel, J.-L. Bourdier and B. Scaillet, Physical conditions, structure and dynamics of a zoned magma chamber: Mt. Pelée (Martinique, Lesser Antilles arc). *J. Geophys. Res.* **107** B5 (2002), pp. 1–28.

Pownceby and O'Neill, 1994. M.I. Pownceby and H.S.t. C. O'Neill, Thermodynamic data from redox reactions at high temperatures. III. Activity composition relations in Ni-Pd alloys from EMF measurements at 850–1250K, and calibration of the NiO+Ni-Pd assemblage as a redox sensor. *Contrib. Mineral. Petrol.* **116** (1994), pp. 327–339.

Robie et al., 1978. R.A. Robie, B.S. Hemingway and J.R. Fisher, Thermodynamic properties of minerals and related substances at 298.15 K and 1 bar (10^5 Pascals) pressure and at higher temperature. *Geol. Surv. Bull.* **1452** (1978), p. 456.

Roeder, 1974. P.L. Roeder, Activity of iron and olivine solubility in basaltic liquids. *Earth Planet. Sci. Lett.* **23** (1974), pp. 397–410.

Roux and Lefèvre, 1992. J. Roux and A. Lefèvre, A fast-quench device for internally heated pressure vessels. *Eur. J. Mineral.* **4** (1992), pp. 279–281.

Roux et al., 1994. J. Roux, F. Holtz, A. Lefèvre and F. Schulze, A reliable high-temperature setup for internally heated pressure vessels: Applications to silicate melt studies. *Am. Mineral.* **79** (1994), pp. 1145–1149.

Scaillet et al., 1992. B. Scaillet, M. Pichavant, J. Roux, G. Humbert and A. Lefèvre, Improvements of the Shaw membrane technique for measurements and control of fH_2 at high temperatures and pressure. *Am. Mineral.* **77** (1992), pp. 647–655.

Scaillet et al., 1995. B. Scaillet, M. Pichavant and J. Roux, Experimental crystallization of leucogranite magmas. *J. Petrol.* **36** (1995), pp. 663–705.

Schumann, 1951. Schumann Jr. R. and Ensio P. J. (1951) Thermodynamic of iron-silicate slag: Slag saturated with gamma iron. *AIME. Trans.* **191,** 401–411

Schwartzendruber, 1984. L.J. Schwartzendruber, The Fe-Ir (iron-iridium) system. *Bull. Alloy Phase Diagrams* **5** (1984), pp. 48–52.

Silver et al., 1989. L.A. Silver, P.D. Ihnger and E. Stolper, The influence of bulk composition on water in silicate glasses. *Contrib. Mineral. Petrol.* **104** (1989), pp. 142–162.

Sisson and Grove, 1993. T.W. Sisson and T.L. Grove, Experimental investigations of the role of water in calc-alkaline differentiation and subduction zone magmatism. *Contrib. Mineral. Petrol.* **113** (1993), pp. 143–166.

Snyder and Carmichael, 1991. D. Snyder and I.S.E. Carmichael, Olivine-liquid equilibria and the chemical activities of FeO, NiO, Fe_2O_3, and MgO in natural basic melts. *Geochim. Cosmochim. Acta* **56** (1991), pp. 303–318.

Snyder et al., 1993. D. Snyder, I.S.E. Carmichael and R.A. Wiebe, Experimental study of liquid evolution in a Fe-rich, layered mafic intrusion: Constraints of Fe-Ti oxide precipitation on the T-fO_2 and T-d path of tholeiitic magmas. *Contrib. Mineral. Petrol.* **113** (1993), pp. 73–86.

Stull and Prophet, 1971. Stull D. R. and Prophet H. (1971) JANAF thermochemical tables. Second Edition. Washington, National Bureau of standard, 1141

Taylor et al., 1992. J.R. Taylor, V.J. Wall and M.I. Pownceby, The calibration and application of accurate redox sensor. *Am. Mineral.* **77** (1992), pp. 284–295.

Thornber et al., 1980. C.R. Thornber, P.L. Roedder and J.R. Foster, The effect of composition on the ferric-ferrous ratio in basaltic liquids at atmospheric pressure. *Geochim. Cosmochim. Acta* **44** (1980), pp. 525–532.

Toplis and Carroll, 1995. M.J. Toplis and M.R. Carroll, An experimental study of the influence of oxygen fugacity on Fe-Ti oxides stability, phase relations, and mineral-melt equilibria in ferro-basaltic systems. *J. Petrol.* **36** (1995), pp. 1137–1170.

Toplis and Carroll, 1996. M.J. Toplis and M.R. Carroll, Differentiation of ferro-basaltic magmas under conditions open and closed to oxygen: Implications for the Skaergaard intrusions and other natural systems. *J. Petrol.* **37** (1996), pp. 837–858.

Woodland and O'Neill, 1997. A.B. Woodland and H.S.t. C. O'Neill, Thermodynamic data for Fe-bearing phases obtained using noble metal alloys as redox sensors. *Geochim. Cosmochim. Acta* **61** (1997), pp. 4359–4366.

Wilke et al., 2002. M. Wilke, H. Behrens, D.J.M. Burkhard and S. Rossano, The oxidation state of iron in silicic melt at 500 MPa water pressure. *Chem. Geol.* **189** (2002), pp. 55–67.

Appendix: Determination of liquid FeO standard properties

Thermodynamic properties of pure liquid FeO (FeO^{liq}) were extracted from a numerical interpretation of the phase relations in the pseudobinary system SiO_2-FeO +/- Fe_2O_3. This system is constrained by the phase diagram of [Bowen and Schairer, 1934] and numerous measurements of FeO^{liq} activities in the liquid (61 metal-silicate equilibria compiling the works of [Schumann, 1951] and [Bodsworth, 1959]. These activity measurements constrain the energetic of iron in the part of the system containing from 60 to 100 wt.% of molten iron oxides (mainly FeO with Fe_2O_3 increasing from $\sim$0 to 13wt.% as total iron oxides increases from 60–100%). Precise extrapolation of the thermodynamic properties of pure FeO^{liq} is thus feasible. The excess Gibbs free energy of the system (G_{xs}) was fitted using Margules formalism with 3 interaction parameters between liquid SiO_2^{liq} and FeO^{liq} and a symmetric Margules formulation describing the interactions between FeO^{liq} and $Fe_2O_3^{liq}$ (see Table hereafter) Table A1. Interactions between SiO_2^{liq} and $Fe_2O_3^{liq}$ were ignored given that the content of $Fe_2O_3^{liq}$ at the liquidus of Si-bearing crystals are negligible and that ferric iron become an important species of the system when silica is present only at very low concentration (see [Bowen and Schairer, 1934]. The optimization was realized using a minimizing function constrained with inequalities allowing but restraining variations of liquidus temperatures of solids (see [Berman and Brown, 1984 and Berman and Brown, 1987] for LAP method). As initial values, the standard state molten wustite was adopted for liquid FeO [Coughlin, 1954] see Table 1). Throughout the minimization, both enthalpy and entropy of formation of liquid FeO were allowed to vary within 20%. The results including the thermodynamic properties of liquid FeO, the interaction parameters defining G_{xs} and the accuracy of the model are given in the following Table for liquid FeO and liquid SiO_2. The evaluated standard state for liquid FeO are very close to the standard state adopted by [Bodsworth, 1959] and [Matsuzaki et al., 1998] but significantly differ from the thermodynamic parameter of liquid wustite (see text and Table 1).

Table A1. Optimization in the system $FeO-SiO_2 \pm Fe_2O_3$. Upper : Gibbs free energy formula of the components used for the thermodynamic optimization of the molten system $SiO_2-FeO \pm Fe_2O_3$. Middle : Stoichiometry of equilibria used and corresponding evaluated component. Lower : Results of optimization.

Reference	Components	ΔG° formation at 1bar, T°K (J/mol)
Coughlin (1954)	Wustite solid	−265020 + 64.8 .(T)
Coughlin (1954)	Wustite liquid	−237156 + 47.64 .(T)
Robie et al (1978)	Si, O_2	
Berman et Brown (1987)	Crystobalite	−898867 + 170.22 .(T)
Berman et Brown (1987)	Tridymite	−902880 + 174.2 .(T)
DeCapitani et Kirschen (1998)	SiO_2 liquid	−891808 + 166.11 .(T)
O'Neill (1987)	Fayalite	−1450800 + 30.26 .(T)

Equilibria	Evaluated Component
$SiO_2^{cristobalite\text{-}tridymite} = SiO_2^{liq}$	SiO_2^{liq}
$Fe_2SiO_4^{fayalite} = 2\ FeO^{liq} + SiO_2^{liq}$	FeO^{liq} & SiO_2^{liq}
$Fe_{0.947}O^{wustite} = 0.947\ FeO^{liq} + (1-0.947)/2\ O_2^{gas}$	FeO^{liq}
$Fe^{metal} + 1/2\ O_2 = FeO^{liq}$	FeO^{liq}

Standard state for FeO^{liq}*		Margules parameters for the excess free energy			
$\Delta H^\circ_{FeO^{liq}*}$	$\Delta S^\circ_{FeO^{liq}*}$	W_{13}	W_{1234}	W_{1223}	W_{1112}
−226244	−42.49	−125350	57419	−16259	−10128

**$Gxs = X_{FeO}^3.X_{SiO2}.W_{1112} + X_{FeO}^2.X_{SiO2}^2.W_{1223} + X_{FeO}.X_{SiO2}^3.W_{1234} + X_{FeO}.X_{Fe2O3}.W_{13}$

At saturation of Fe, wustite, cristobalite, tridymite, fayalite:

Average difference between measured-calculated chemical potentials (μ_{FeO}^{liq}, μ_{SiO2}^{liq}): 645 J/mol.